Renewable and Sustainable Energy Reviews 241 (2026) 117225

Contents lists available at ScienceDirect

Renewable and Sustainable Energy Reviews

journal homepage: www.elsevier.com/locate/rser

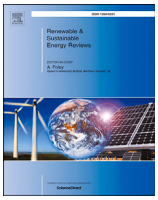

Influence of different aging pathways on the thermal runaway characteristics of lithium-ion batteries: A review with gas evolution as the bridging perspective

Mengying Wang [a], Shaoyan Liu [b], Dong Han [a,c], Zhen Huang [a,c], Jiabo Zhang [a,c,*]

[a] Key Laboratory for Power Machinery and Engineering, Ministry of Education, Shanghai Jiao Tong University, Shanghai 200240, China
[b] Department of Mechanical Engineering, The Pennsylvania State University, University Park, PA 16802, USA
[c] Shanghai Non-carbon Energy Conversion and Utilization Institute, Shanghai 200240, China

HIGHLIGHTS

- Gas evolution is used as a bridge between aging pathways and thermal runaway risks.
- Aged gas under high/low temperatures, high C-rate, and overcharge/discharge is summarized.
- Thermal safety characteristics are summarized across different aging pathways.
- Indicator gases are reviewed for aging diagnosis and safety assessments.
- Machine learning applications in gas-based early warning strategies are discussed.

ARTICLE INFO

Keywords:
Lithium-ion batteries
Gas evolution
Aging diagnosis
Thermal runaway
Early warning
Data-driven methods

ABSTRACT

Lithium-ion batteries (LIBs) are increasingly used in electric vehicles and large-scale energy storage systems. However, their long-term operational safety remains a critical bottleneck, especially as batteries experience progressive aging during extended service. This review examines how primary aging pathways, including high temperature, low temperature, high C-rate cycling, and overcharge/over-discharge conditions, affect aging reactions and consequently influence thermal runaway (TR) behavior. Specifically, these aging pathways trigger different side reactions and produce characteristic gas signals, such as hydrogen, carbon oxides, and hydrocarbons. These gas signals can reflect the internal aging state of batteries and help explain changes in TR characteristics and overall thermal safety behavior. As the relationship among aging pathways and TR characteristics is strongly path-dependent, gas evolution is reviewed here as a bridge linking aging mechanisms with thermal safety assessment. Moreover, the review further examines how gas signals can be integrated with machine learning methods to support TR diagnosis and early warning. This combined perspective helps improve the safety design and operation of LIBs.

1. Introduction

With the transition to cleaner energy systems, lithium-ion batteries (LIBs) have become an important and rapidly growing part of modern power systems [1]. Grid-scale energy storage batteries and electric vehicle power batteries are commonly designed to last 10 years or longer [2,3]. However, maintaining safety over long service periods remains difficult. As batteries age, degradation of battery components reduces thermal stability, making long-term safety a major challenge for their deployment [4]. Recent fire incidents characterized by thermal runaway (TR) also highlight the need for stronger safety management across the full life cycle [5,6].

While fresh LIBs initially meet stringent performance standards, continuous operation inevitably leads to complex internal changes. Compared with fresh batteries with relatively well-defined electrochemical states, aged LIBs undergo different aging pathways throughout their service life [7,8]. During these processes, side reactions are triggered with characteristic gaseous byproducts generated. For example, high-temperature exposure accelerates the decomposition of the electrolyte

* Corresponding author at: Key Laboratory for Power Machinery and Engineering, Ministry of Education, Shanghai Jiao Tong University, Shanghai 200240, China.
Email address: zhangjiabo@sjtu.edu.cn (J. Zhang).

https://doi.org/10.1016/j.rser.2026.117225
Received 11 March 2026; Received in revised form 29 May 2026; Accepted 22 June 2026

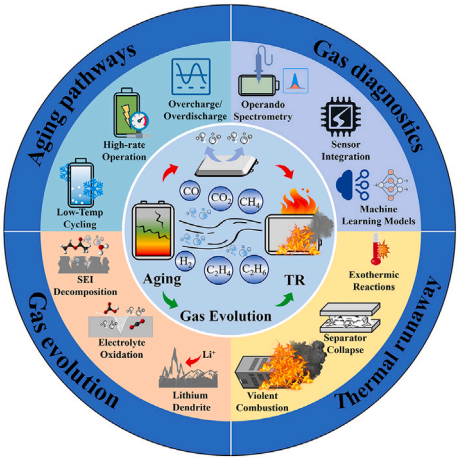

Fig. 1. Gas evolution links aging pathways with TR hazards and diagnostic strategies.

and solid electrolyte interphase (SEI), leading to gases such as CO_2 and CO [9,10]. In contrast, low-temperature operation and high C-rate cycling both promote lithium plating on the anode. The plated lithium can then react with residual moisture and other reactive species, leading to H_2 generation [11,12]. Overcharge can drive lattice oxygen release, electrolyte oxidation, and lithium plating, leading to mixed gas products such as carbon oxides, H_2, and hydrocarbons [13]. These gas evolution characteristics can serve as useful chemical indicators of the underlying aging mechanisms and help assess the internal state of LIBs [14,15].

On the other hand, the above aging pathways and gas generation could further influence battery safety [16]. Specifically, distinct aging mechanisms modify the TR initiation threshold by altering electrode/electrolyte interfacial conditions [17]. For example, LIBs exhibiting severe lithium plating after low-temperature operation display significantly reduced self-heating onset temperatures compared with fresh batteries, whereas those dominated by high temperature calendar aging may in some cases show elevated onset temperatures due to material loss [18,19]. Recent aging-pathway studies further show that thermal hazards can differ even when batteries are compared at similar usable capacity, confirming that safety evolution depends on aging pathways rather than state of health (SOH) alone [20,21]. These observations suggest that aging pathways, gas evolution, and thermal safety are strongly coupled throughout the battery cycle life, yet accurately characterizing their interactions remains challenging [22,23].

To improve the safety of aging LIBs, extensive efforts have been devoted to understanding aging mechanisms, elucidating gas-generation pathways, developing diagnostic and early-warning methodologies, and establishing thermal-hazard mitigation and control strategies [24–26]. However, the links among them are still largely unclear. To address this gap, gas evolution is considered as the central link between battery aging and thermal safety. As illustrated in Fig. 1, this review summarizes how major aging pathways, including temperature-driven degradation, cycling-induced aging, and overcharge/over-discharge conditions, influence gas evolution and ultimately affect TR behavior. The roles of key gaseous species such as CO_2, H_2, O_2, and C_2H_4 are discussed in linking degradation processes to thermal safety evolution. In addition, the coupling between gas indicators and TR characteristics is examined for aging diagnosis and risk interpretation, including recent machine-learning approaches. Finally, in-depth insights are summarized together with future research directions.

2. Gas evolution mechanisms during aging

The performance deterioration of LIBs accelerates under critical operating conditions including high temperature, low temperature, high C-rate cycling, and overcharge or over-discharge scenarios [27]. Distinct aging pathways trigger specific side reactions leading to characteristic gas generation behaviors [28]. High temperature exposure mainly promotes the thermal decomposition of electrolyte solvents yielding CO_2 and hydrocarbon species [29]. In contrast, low-temperature environments and high C-rate cycling induce lithium plating on graphite anodes which leads to substantial H_2 evolution [11]. Furthermore, overcharge conditions drive electrolyte oxidation and cathode lattice destabilization, leading to carbon oxide generation and lattice oxygen release [13,30]. Consequently, the specific composition and volume of these gases act as critical indicators for identifying underlying aging mechanisms [31]. This section summarizes the correlations between aging pathways and specific gas signatures and highlights how gas analysis serves as an effective tool for assessing SOH and diagnosing aging mechanisms. Because the interpretation of gas signatures depends strongly on how the gases are measured, the main experimental approaches are first summarized.

Operando techniques such as online electrochemical mass spectrometry (OEMS) and differential electrochemical mass spectrometry (DEMS) offer high temporal resolution, enabling the tracking of gas onset and evolution, which helps correlate gas release with electrochemical events [32,33]. Nevertheless, challenges remain in multicomponent systems due to species overlap and calibration difficulties. Moreover, methods based on gas chromatography (GC) typically provide better species resolution. Gas chromatography-mass spectrometry (GC-MS) is particularly effective for molecular identification, while gas chromatography flame ionization detection (GC-FID) and gas chromatography-thermal conductivity detection (GC-TCD) are advantageous for quantifying hydrocarbons or screening permanent gases [10,34,35]. However, these methods are generally less suited for continuous real-time monitoring. In this context, Fourier transform infrared spectroscopy (FTIR) is well-suited for analyzing externally vented gases owing to its rapid response and ease of implementation for targeted species [15,36]. Similarly, in-situ Raman spectroscopy shows promise for real-time, non-destructive molecular-level gas analysis directly within the battery environment [37]. Compared to GC-MS, operando Raman provides immediate mechanistic guidance during the dynamic degradation process, though it currently still encounters practical constraints such as weak signal intensity, complex optical-path configuration, and calibration issues in multicomponent gas mixtures. Dedicated gas sensors are more appropriate for engineering-level monitoring and early warning due to their fast response and ease of deployment, yet they typically offer less mechanistic insight compared to spectroscopic or chromatographic techniques [31,38]. Together, these complementary techniques form the practical foundation for interpreting the gas signatures discussed in the following sections.

2.1. Gas evolution characteristics under various aging conditions

External operating conditions such as temperature and charging protocols significantly influence the aging process of LIBs. These stress factors accelerate specific side reactions at the electrode interface and lead to distinct gas generation behaviors [39]. Therefore, specific gas components serve as direct indicators for identifying internal aging mechanisms [31,33]. This section summarizes gas evolution characteristics under representative aging scenarios to provide a basis for battery health monitoring.

2.1.1. Influence of high temperatures on gas evolution

The primary side reactions during high-temperature aging involve the thickening of the SEI layers, decomposition of the electrolyte, and structural degradation of the cathode materials, accompanied by the generation of gases such as CO_2, C_2H_6, CH_4, and CO [39,40]. At elevated temperatures, the SEI layers become thermally unstable, undergoing partial dissolution and decomposition. The consequently exposed graphite anode surface initiates reduction reactions with the electrolyte, leading to continuous SEI thickening [41]. Simultaneously,

under combined high-temperature and high-voltage conditions, the oxidative stability of the electrolyte at the cathode surface deteriorates, accelerating oxidative decomposition of electrolytes [42]. Furthermore, elevated temperatures exacerbate transition metal dissolution from the cathode material, enabling these metal ions to migrate to the anode, where they compromise SEI integrity and catalyze further electrolyte decomposition [39].

The origin of these gases depends heavily on battery voltage and electrode stability [43]. Hall et al. [44] showed that gas volume at 4.2 V is substantially higher than at 2.5 V during 60 °C storage. This confirms that cathode-side reactions become more important under high-voltage conditions. A key question is whether the resulting gas evolution is driven mainly by electrochemical solvent oxidation or by reactive oxygen species released from the cathode. Strehle et al. [45] systematically compared $LiNi_xCo_yMn_zO_2$ (NCM) LIBs aged at 22 °C and 45 °C. It was found that cycling at 45 °C more than doubled the capacity fade rate and led to the formation of a much thicker rock-salt-like reconstruction layer on the cathode surface, increasing from ~6 nm at 22 °C to ~12–14 nm at 45 °C. The observed surface reconstruction is associated with, and likely initiated by, lattice oxygen release at high SOC. According to new theoretical and experimental insights by Spotte-Smith et al. [46] and Chang et al. [47], this released oxygen often exists as highly reactive singlet oxygen ($^1O_2$) or radical anions. These species chemically attack the carbonate solvents, rapidly generating CO_2 and CO rather than simple thermal decomposition.

Simultaneously, the anode SEI becomes dynamically unstable at high temperatures. Taskovic et al. [50] observed that NCM523 batteries produced significantly more gas at 40 °C than at 20 °C due to enhanced parasitic reaction kinetics [28]. The specific gas composition reveals the degradation pathways. As shown in Fig. 2(a), Li et al. [11] detected CO_2, H_2, CO, and alkanes in $LiNi_xCo_yAl_zO_2$ (NCA) batteries cycled at 45 °C, linking CO_2 formation partly to the decomposition of the fluoroethylene carbonate (FEC) additive. However, the dominant gas species remains a subject of debate. Guillot et al. [51] found that CO was the most abundant gas generated during 60 °C storage of graphite/NCM622 pouch batteries. In contrast, Zhang et al. [52] reported that H_2 accounted for over 50% of the total gas in NCM631 batteries cycled at 60 °C. The unexpected H_2 generation is attributed to the reduction of protonated solvents and water decomposition catalyzed by transition metals. This apparent discrepancy among reported dominant gases can be partly explained by electrode crosstalk, in which degradation products formed at one electrode migrate to the counter electrode and undergo further reactions. Xiong et al. [53] demonstrated this using physically separated pouch batteries. The pouch containing only a delithiated cathode generated significant CO_2, while the full battery produced much less. This indicates that oxidative gases generated at the cathode diffuse to the anode and are consumed there. Additionally, dissolved transition metal ions can migrate from the cathode to the anode. These ions act as catalysts for electrolyte decomposition on the anode surface, further altering the total gas volume and composition [54].

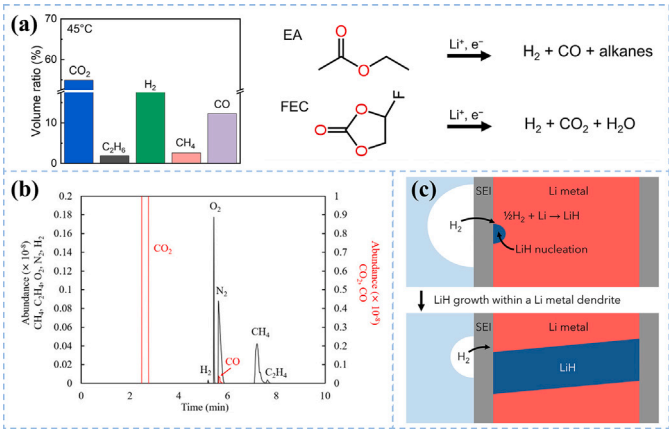

Fig. 2. Schematic diagram contrasting gas evolution mechanisms under high/low temperature aging. (a) Composition analysis and reaction pathways for $LiNi_xCo_yAl_zO_2$ (NCA) pouch batteries cycled at 45 °C [11]. (b) Mechanism of gas generation arising from the corrosion of deposited lithium under low temperature conditions [48]. (c) Formation process of LiH dendrites via the reaction between evolved H_2 and metallic lithium [49].

The aging pathway also dictates the gassing behavior. High-temperature storage (calendar aging) is primarily a chemical process driven by thermodynamic instability. Kim et al. [55] noted that initial gas generation during storage often originates from residual surface impurities like Li_2CO_3. In contrast, cycling aging introduces mechanical stress. Zhang et al. [39] compared NCM631 batteries under both storage and cycling at 60 °C. Remarkably, they identified H_2 as the dominant gas species (≥ 60%) in both modes, originating from the reduction of protic electrolyte oxidation species ($R-H^+$). In addition, the continuous volume expansion induces particle cracking, exposing fresh active surfaces that accelerate reactions with electrolytes. Crucially, the rapid gas generation consumes the electrolytes, causing localized drying of the anode. This drying disrupts the potential distribution, triggering localized lithium plating upon recharging. The highly reactive plated lithium then reacts with the electrolyte, leading to severe gas evolution of H_2.

2.1.2. *Influence of low temperatures on gas evolution*

In contrast to the thermodynamically driven decomposition at elevated temperatures, low-temperature aging is primarily dominated by sluggish reaction kinetics and impeded ion transport [56]. Under low-temperature conditions, the sluggish solid-state diffusion of Li^+ within the graphite anode induces severe concentration polarization. This causes the anode potential to rapidly decline below 0 V (vs. Li/Li^+), thereby inducing lithium plating [57,58]. The formation of plated lithium represents the most severe gas-generating side reaction during low-temperature aging, serving as the fundamental cause of gas evolution. Unlike stable intercalated lithium, the deposited metallic lithium exhibits exceptionally high chemical reactivity and initiates distinct gassing pathways. The direct reduction of trace moisture or protonated species by the active metallic surface evolves H_2, a characteristic signature of lithium plating [11,59]. Furthermore, the mechanical embrittlement of the SEI at low temperatures, coupled with the stress of dendrite growth, leads to continuous SEI rupture [60,61]. Subsequently, the exposed reactive metallic lithium instantly reduces the electrolyte solvents, releasing C_2H_4 and forming a new SEI layer [60]. Ultimately, the regenerated SEI layers cover the metallic lithium to form electrochemically inactive dead lithium, thereby causing irreversible capacity loss.

Quantitative evidence further suggests that severe gas evolution accompanies lithium plating/corrosion under kinetic limitations at low temperatures. Ng et al. [48] reported pronounced gassing in NCM532/graphite batteries cycled at −29 °C, with detected species including H_2 and C_2H_4. As illustrated in Fig. 2(b), these gases are closely associated with the high reactivity of plated lithium and the ensuing electrolyte decomposition. Xiang et al. [62] showed that the reductive decomposition of ethylene carbonate (EC) during Li deposition continuously releases C_2H_4, providing a gaseous signature of ongoing side reactions on metallic lithium and contributing to gas-induced inactive Li formation.

Although H_2 is traditionally attributed to moisture reduction, Vilá et al. [49] utilized cryogenic electron microscopy (Cryo-EM) to demonstrate that it actively reacts with plated lithium to generate LiH (Fig. 2(c)). This finding is thermodynamically supported by Xu et al. [63], who described the equilibrium between metallic Li and H_2. The formation of highly insulating LiH not only consumes active lithium inventory but also electrically isolates the deposits, rendering them “dead” and accelerating capacity fade.

Unlike high-temperature aging where reactions typically slow down upon resting, low-temperature aging exhibits a delayed hazard. Wang et al. [64] observed that batteries subjected to low-temperature cycling continued to generate significant gas volumes when subsequently stored at 25 °C. This phenomenon indicates that the plated lithium retains high chemical activity and continues to corrode the electrolyte during the warming or resting phase, highlighting a latent safety risk.

2.1.3. Influence of charging rates on gas evolution

Charging rate strongly changes both the degradation pathway and the resulting gas-evolution behavior. At relatively low charging rates, kinetic polarization is limited, so gas generation is more strongly governed by voltage-dependent parasitic reactions and the time spent at elevated SOC. By contrast, high charging rates increase electrode overpotential and Li-concentration heterogeneity, thereby promoting rate-induced degradation processes such as lithium plating, repeated SEI rupture/regrowth, and mechanically driven electrode damage. These accelerated side reactions intensify gas evolution and can also modify the dominant gas species released during charging [65–67].

Battery aging under low C-rate conditions exhibits calendar-aging-like characteristics, because the extended cycle duration increases the residence time at elevated voltage and prolongs electrode-electrolyte contact. This prolonged exposure allows slow parasitic reactions and interphase growth to accumulate over time. Consequently, continuous SEI growth on the anode can promote ongoing electrolyte side reactions and low-level gas generation [68]. In this regime, gas evolution is generally more gradual and is more strongly governed by voltage- and time-dependent parasitic reactions than by rate-induced polarization. The evolved gas is therefore often dominated by CO_2, together with smaller amounts of light hydrocarbons, consistent with relatively mild interfacial degradation [67].

In contrast, high C-rate cycling introduces significant mechanical strain induced by volume expansion. The rapid insertion of lithium ions creates large concentration gradients within the active particles. This inhomogeneity is associated with particle micro-cracking [69]. These cracks expose fresh anode surfaces to the electrolyte. Electrolyte solvents undergo rapid reduction on these exposed fresh surfaces. This process triggers a surge in unsaturated hydrocarbons, particularly C_2H_4, which serves as a distinct signature of high-rate aging [70].

Kinetic polarization at high rates often induces lithium plating side reactions. Metallic lithium deposits on the anode surface when the potential drops below 0 V [71]. This deposited metallic lithium has a high specific surface area and reacts with the electrolyte, producing H_2 and consuming electrolyte [11,72]. Additionally, the Joule heating raises the internal battery temperature during fast charging. High temperatures accelerate the thermal decomposition of metastable species, leading to increased generation of CO [9].

As mentioned above, H_2 is generated through several reaction pathways depending on the aging condition [32]. Therefore, it is helpful to summarize how it is generated [52]. Specifically, the highly active metallic surface of deposited lithium creates an extremely reductive environment. This freshly deposited lithium reacts vigorously with the bulk carbonate electrolyte while simultaneously serving as the primary site for the direct reduction of trace moisture and protonated species [32]. Under low-temperature charging, the dominant trigger is transport-limited lithium plating [11]. During high-rate cycling, current-dependent polarization remains the critical driver for lithium plating, while the subsequent H_2 generation kinetics are further accelerated by interphase rupture, fresh surface exposure, and Joule heating [31,66,71]. In overcharge conditions, H_2 generation is jointly governed by voltage-driven electrode imbalance and polarization [73]. Even during high-temperature aging, H_2 evolution can become significant when protic species, formed through crosstalk or solvent oxidation, are continuously reduced at the anode [39]. Therefore, a comprehensive understanding of H_2 evolution requires distinguishing common reactive intermediates, such as freshly deposited lithium or catalytically activated anode surfaces, from the specific kinetic drivers unique to each aging pathway.

As a result, the charging rate influences the relative importance of different degradation pathways. Lower rates generally allow interfacial passivation-related side reactions to accumulate over time, whereas higher rates more readily intensify mechanically coupled degradation processes. Accordingly, differences in gas composition may provide useful non-destructive clues to the underlying aging behavior. During calendar aging, gas accumulation during storage reflects time-dependent parasitic reactions, and CO_2 can be a major component of the evolved gas [74]. By comparison, C_2H_4 is often associated with EC reduction and anode interfacial reactions related to SEI formation or regeneration [28]. Understanding these relationships can help guide battery-management strategies under different operating conditions.

2.1.4. Influence of overcharge and over-discharge on gas evolution

Overcharge and over-discharge, as the primary forms of electrical stress [75], drive the electrode potentials beyond the thermodynamic stability window of the electrolyte, significantly accelerating battery aging. Given that these side reactions are inherently dependent on electrode potential, overcharge and over-discharge aging induce distinct gas evolution [76,77].

During overcharge, excessive lithium extraction can destabilize the cathode crystal structure [30]. At sufficiently high overcharge voltages, pronounced electrolyte decomposition can occur and is accompanied by reduced cathode stability [78]. Ohsaki et al. [73] showed that CO_2 is a major gas species generated during overcharge, consistent with oxidative decomposition reactions at highly delithiated cathode surfaces. Gas evolution, however, should not be attributed solely to electrolyte oxidation, but is also closely related to the structural stability of the cathode material [30]. Jung et al. [79] showed that the onset of pronounced CO_2 and CO evolution coincides with the release of lattice oxygen from layered NCM cathodes. Their results further suggest that reactive oxygen species released at high states of delithiation chemically react with the electrolyte and contribute substantially to the observed gas evolution. Furthermore, the specific gas signature serves as a diagnostic probe for the oxidation capacity of the cathodes. Kong et al. [80] identified C_2H_2 as a characteristic indicator that is inversely correlated with oxidation capacity. They found that cathodes with weaker oxidation capacity (e.g., $LiFePO_4$) generate more C_2H_2, whereas strong oxidizers like $LiCoO_2$ mainly generate CO_2.

In addition, the amount of gas generated during the overcharge aging is heavily dependent on the cutoff voltage. Mao et al. [81] observed that raising the upper cutoff voltage significantly intensifies gas generation. Crucially, they highlighted the crosstalk effect in which gases generated at the cathode (such as CO_2 and fluorinated alkanes) migrate to the anode, where they are subsequently consumed, leading to the depletion of gaseous products during overcharge cycling. Furthermore, recent advancements have highlighted that this gas evolution is dynamically modulated by the aging pathways rather than static voltage thresholds. Guo et al. [82] demonstrated that the kinetics of gas generation under high-temperature-coupled overcharge conditions are non-linearly coupled with the C-rates. Under high-rate conditions (e.g., 1.5 C), the accumulation of Joule heat and polarization accelerates the onset of electrolyte decomposition. Consequently, the gas pressure buildup is no longer dictated solely by voltage (under quasi-equilibrium low-rate conditions) but is increasingly driven by the internal TR kinetics. This implies that the gas indicator of overcharge cycling is a joint effect of both the voltage window and C-rates.

In contrast, over-discharge aging is characterized by the dissolution of the copper current collector and the decomposition of the SEI layers. While early established mechanisms emphasized the generation of hydrocarbons (e.g., CH_4, C_2H_6) resulting from SEI reduction during over-discharge cycling [83,84], recent investigations have refined this understanding. Ouyang et al. [77] showed that severe over-discharge increases the anode potential, causing the copper current collector to

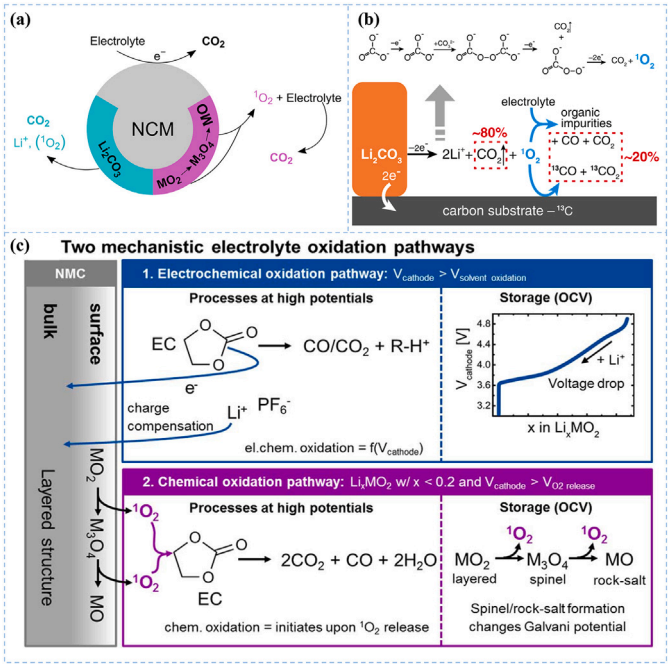

Fig. 3. Gas generation at the cathode: (a) Schematic diagram of representative CO2-evolution pathways at Ni-rich NCM cathodes [96]. (b) Schematic diagram of Li_2CO_3 decomposition during charging [97]. (c) Schematic diagram of electrochemical and chemical electrolyte oxidation at elevated potentials [79].

oxidize first to Cu^+ and then to Cu^{2+}. Part of the dissolved copper species migrates to the cathode side and is reduced to metallic copper, forming dendrites that can penetrate the separator and induce internal short circuits (ISC). Moreover, alongside this severe physical degradation, over-discharge triggers intense exothermic side reactions and the massive release of combustible gases.

2.2. Chemical degradation mechanisms of battery components

Degradation in LIBs primarily originates from parasitic side reactions and the structural deterioration of electrode materials. As the working potentials of high-energy electrodes frequently extend beyond the thermodynamic stability window of the electrolyte, interfacial decomposition becomes unavoidable [85]. These oxidative and reductive processes involve gas generation and lead to loss of lithium inventory (LLI), loss of active material (LAM), and continuous impedance growth [86]. Moreover, soluble species generated at one electrode can diffuse to the counter-electrode and trigger self-amplifying chemical crosstalk [87].

2.2.1. Oxidative decomposition and structural instability at the cathode

The cathode plays a key role in determining the energy density of LIBs and can make a major contribution to gas evolution during aging. As illustrated in Fig. 3(a), cathode-side gas generation is generally associated with surface impurity decomposition (e.g., Li_2CO_3), electrolyte oxidation, and, for layered oxide cathodes at high SOC, lattice-oxygen-related degradation. The main reactions involved in cathode-side gas generation are summarized in Table 1. For layered transition metal oxides such as $LiCoO_2$ (LCO) and NCM, structural stability is compromised at high SOC, promoting lattice-oxygen activation and release (Reactions R1–R4) [79,88]. This process is especially severe for Ni-rich cathodes, stemming from the reduced covalency of Ni-O bonds which lowers the energy barrier for oxygen release.

Surface side reactions on the cathode constitute another primary pathway for gas generation. During battery manufacturing and storage,

Table 1
Gas generation reactions of LIBs during aging.

Reaction	No.	Ref.
Cathode Reactions		
$2\,Li_0FePO_4 \rightarrow Fe_2P_2O_7 + \frac{1}{2}\,O_2$	R1	[89]
$Li_xCoO_2 \rightarrow \frac{1-x}{3}\,Co_3O_4 + x\,LiCoO_2 + \frac{1-x}{3}\,O_2$	R2	[90]
$3\,MO_2$ (layered) $\rightarrow M_3O_4$ (spinel) $+ O_2$	R3	[91]
M_3O_4 (spinel) $\rightarrow 3\,MO$ (rock−salt) $+ \frac{1}{2}\,O_2$	R4	[91]
$2\,Li_2CO_3 \rightarrow 4Li^+ + 4e^- + 2\,CO_2 + {}^1O_2$	R5	[59]
$LiPF_6 + H_2O \rightarrow LiF + POF_3 + 2\,HF$	R6	[92]
$Li_2CO_3 + 2\,HF \rightarrow 2LiF + H_2O + CO_2$	R7	[93]
$2\,Li_2CO_3 + LiPF_6 \rightarrow LiPO_2F_2 + 4\,LiF + 2\,CO_2$	R8	[94]
$LiOH + Li^+ + e^- \rightarrow Li_2O + \frac{1}{2}\,H_2$	R9	[95]
$EC \rightarrow C_3H_2O_3$ (VC) $+ 2\,H^+ + 2\,e^-$	R10	[59]
$Li_2CO_3 + 2\,H^+ \rightarrow 2Li^+ + CO_2 + H_2O$	R11	[96]
$2\,{}^1O_2 + C_3H_4O_3$(EC) $\rightarrow 2CO_2 + CO + 2\,H_2O$	R12	[79]
$(1-\frac{x}{2})\,{}^1O_2 + C \rightarrow (1-x)\,CO_2 + x\,CO$	R13	[97]
Anode Reactions		
$LiOH + ROCO_2R \rightarrow ROCO_2Li + ROH$	R14	[55]
$2\,ROCO_2Li + H_2O \rightarrow Li_2CO_3 + 2\,ROH + CO_2$	R15	[55]
$2\,EC + 2\,Li^+ + 2\,e^- \rightarrow C_2H_4 + (LiOCOOCH_2)_2$ (LEDC)	R16	[98]
$C_3H_6O_3$(DMC) $+ 2\,Li^+ + 2\,e^- \rightarrow CO + 2\,CH_3OLi$	R17	[73]
$H_2O + e^- \rightarrow OH^- + \frac{1}{2}\,H_2$	R18	[99]
$OH^- + EC \rightarrow HO{-}CH_2{-}CH_2{-}OH + CO_2$	R19	[100]
$LiPF_6 \rightarrow LiF + PF_5$	R20	[101]
$PF_5 + H_2O \rightarrow POF_3 + 2\,HF$	R21	[102]
$LiOCO_2R + HF \rightarrow LiF + ROH + CO_2$	R22	[103]
$Li_2CO_3 + 2\,HF \rightarrow 2LiF + H_2O + CO_2$	R23	[104]
$ROCO_2R + Li_2CO_3 + 2\,HF \rightarrow 2LiF + 2\,ROH + 2\,CO_2$	R24	[55]
$LiOH + HF \rightarrow LiF + H_2O$	R25	[105]
$LEDC + 2\,HF \rightarrow 2LiF + 2\,CO_2 + EG$	R26	[106]
$HF + Li^+ + e^- \rightarrow \frac{1}{2}\,H_2 + LiF$	R27	[107]
$C + 2\,H_2O \rightarrow CO_2 + 4\,H^+ + 4\,e^-$	R28	[108]
$C + H_2O \rightarrow CO + 2\,H^+ + 2\,e^-$	R29	[100]
Crosstalk Reactions		
$LEDC + Mn^0 \rightarrow Li_2CO_3 + C_2H_4 + MnCO_3$	R30	[109]
$2\,CO_2 + 2\,Li \rightarrow Li_2C_2O_4$	R31	[34]
$Li_2C_2O_4 \rightarrow 2CO_2 + 2\,Li^+ + 2\,e^-$	R32	[34]

residual lithium compounds such as Li_2CO_3 and LiOH inevitably accumulate on the cathode surface, where they can react with the $LiPF_6$ salt or directly catalyze solvent decomposition. These surface alkaline impurities, which are mainly Li_2CO_3, generate gas through direct decomposition into O_2 and CO_2 during charging (R5). Otherwise, they react with HF derived from the hydrolysis of $LiPF_6$ by trace moisture to generate LiF and CO_2 (R6-R7). Li_2CO_3 can also react with $LiPF_6$ to yield CO_2 (R8). Additionally, surface LiOH is electrochemically reducible to Li_2O and H_2 (R9). To clarify the specific pathways, Song et al. [59] investigated the chemical decomposition pathway of residual lithium carbonate on cathode surfaces using OEMS and GC. The results showed that CO_2 evolution increased with the population of free EC near the cathode surface. Linear sweep voltammetry indicated anodic dehydrogenation of free EC, while proton nuclear magnetic resonance (^1H NMR) identified vinylene carbonate (VC) as the dehydrogenation product, indicating that free EC can release protons through the De-H EC pathway (R10). These protonic species subsequently react with residual Li_2CO_3, triggering its chemical decomposition and CO_2 release (R11). Separately, Jung et al. [79] proposed that reactive lattice oxygen released from layered oxide cathodes can chemically oxidize EC to form CO_2, CO, and H_2O (R12). Cao et al. [97] employed an in situ differential electrochemical mass spectrometry-gas chromatography (DEMS-GC) coupled system to quantify gas evolution during the electrochemical oxidation of lithium carbonate on carbon substrates. As illustrated in Fig. 3(b), the decomposition of Li_2CO_3 accounted for the majority of CO_2 release (~80%), whereas the decomposition of the carbon substrate and electrolyte contributed the remaining 20% (R13).

Furthermore, the oxidative decomposition of electrolytes on the cathode surface constitutes another critical source of gas evolution [110]. This decomposition generally proceeds through two pathways,

namely electrochemical oxidation and chemical oxidation [46,111]. At sufficiently high cathode potentials, electrolyte oxidation can contribute to CO_2 evolution, and its extent depends on the applied potential and the interfacial reactivity of the cathode/electrolyte system [112]. When the battery is charged to high voltages beyond the oxidative stability window of the electrolyte, carbonate solvents such as EC can undergo anodic oxidation at the cathode interface, generating CO_2, CO, and trace hydrocarbon gases, while also promoting the formation and continuous reconstruction of an unstable cathode electrolyte interphase (CEI) [110,113]. In contrast, chemical oxidation is driven by highly reactive lattice oxygen species, especially singlet oxygen, which react with carbonate solvents to produce CO_2, CO, and H_2O [79,114]. Therefore, the key to distinguishing these two mechanisms is whether gas evolution is governed primarily by electrode potential or by oxygen release from the cathode lattice. Recent studies increasingly suggest that, for layered oxide cathodes, gas evolution is more closely associated with the degree of delithiation and oxygen release than with the nominal applied voltage alone [79,114].

To validate this mechanism, Jung et al. [79] utilized OEMS to reveal that the onset potentials of CO_2 and CO evolution during NCM charging coincide closely with the release of lattice oxygen ($^1O_2$) (Fig. 3(c)). Complementing these findings, Wandt et al. [114] provided unequivocal spectroscopic evidence for this pathway by detecting the characteristic photon emission of singlet oxygen during NCM delithiation. Their work demonstrated that the evolution of these reactive oxygen species is governed by the SOC rather than the operating potential and directly triggers the simultaneous chemical degradation of the electrolyte. To further decouple the contributions of electrochemical and chemical oxidation, Jung et al. [113] compared NCM111, NCM622, NCM811, $LiNi_{0.5}Mn_{1.5}O_4$ (LNMO), and pure conductive carbon electrodes. They showed that the onset potentials of CO_2 and CO evolution depend strongly on the electrode material, following the order NMC811 < NMC111 ≈ NMC622 < conductive carbon ≈ LNMO. This trend indicates that, for NMC cathodes, substantial electrolyte decomposition can occur in a lower voltage window than on conductive carbon, consistent with a chemically driven pathway associated with oxygen release, whereas electrolyte oxidation on conductive carbon becomes significant only above about 5.0 V [79,113]. Accordingly, within practical operating voltages of layered NCM cathodes, electrolyte decomposition is better described as being dominated by chemical oxidation triggered by oxygen release rather than by purely electrochemical anodic oxidation.

2.2.2. Reductive decomposition and SEI evolution at the anode

Gas evolution at the anode side is primarily attributed to the formation and evolution of the SEI during initial cycles, alongside side reactions involving trace moisture. During the initial charge/discharge process, once the anode potential drops below the reduction potential of the electrolytes, solvent molecules (e.g., EC) and electrolyte salts ($LiPF_6$) undergo reductive decomposition, establishing a thin, compact passivation layer known as the SEI. As illustrated in Fig. 4(a), the SEI comprises not only metastable organic compounds, such as lithium alkyl carbonates ($ROCO_2Li$) and lithium ethylene dicarbonate (LEDC), but also thermodynamically stable, dense inorganic components like Li_2CO_3 [115–117]. Representative EC-reduction pathways yielding lithium alkyl dicarbonates and Li_2CO_3 have been reported previously [118]. In addition, possible secondary reactions involving LiOH and carbonate solvents are shown in R14–R15 [55]. This formation and transformation process entails the irreversible consumption of active lithium inventory and electrolyte, accompanied by substantial gas generation, mainly C_2H_4 and CO (R16–R17) [119]. Although the SEI layer is designed to passivate the anode surface, gas evolution does not cease after formation but accumulates throughout the long-term aging process. This is largely driven by the significant volumetric fluctuations of the anode material during cycling, which induce mechanical stress and fracture the SEI layer. The subsequent exposure of fresh active surfaces to the electrolyte triggers SEI regeneration and the continuous evolution of

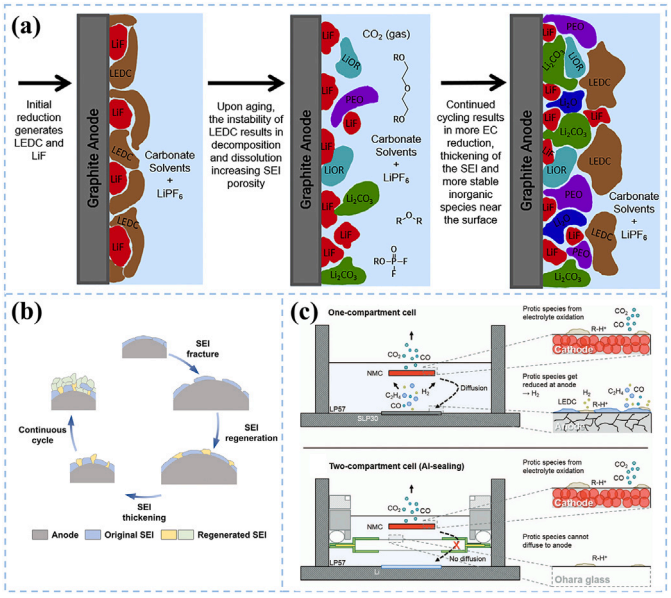

Fig. 4. (a) SEI thickening and compositional changes during aging [115]. (b) Schematic illustration of the fracture and subsequent regeneration of the SEI layer during cycling [120]. (c) Schematic of $R-H^+$ diffusion from cathode to anode [32].

reductive gases, primarily C_2H_4 and CO (Fig. 4(b–c)). For silicon-based anodes, this stress-induced solvent reduction is notably exacerbated by the drastic volumetric expansion of silicon particles.

Beyond SEI degradation and regeneration, residual trace water in the electrolyte acts as a critical impurity and a key chemical trigger for gas evolution. The impact of trace moisture operates through two main mechanisms: direct reductive decomposition and a chain reaction initiated by lithium salt hydrolysis. Specifically, trace water can be reduced at low anode potentials to generate H_2 (R18), while the resulting hydroxide species may further promote EC hydrolysis and carbonate-solvent decomposition, contributing to CO_2 evolution (R19) [99,121]. More critically, trace moisture induces the hydrolysis of $LiPF_6$ to form HF (R20–R21). HF not only corrodes SEI components but also catalyzes the cationic ring-opening polymerization of carbonate solvents, producing various gaseous products including CO_2 (R22–R27). This autocatalytic process can accelerate electrolyte failure. Bernhard et al. [99] employed OEMS to quantitatively confirm that ppm-level trace water is a primary source of early-stage gassing. Compared to an anhydrous electrolyte (<20 ppm), a system containing 4000 ppm water exhibited a surge in H_2 evolution from ~250 ppm to ~8000 ppm during the first cycle in graphite half-batteries. Beyond direct water reduction, cathode-to-anode crosstalk represents another critical pathway for H_2 generation. Metzger et al. [32] utilized a specialized two-compartment battery (Fig. 4(c)) to decouple these interactions. They observed negligible H_2 evolution in diffusion-restricted half-batteries, whereas substantial H_2 was released in full batteries, confirming that anodic H_2 evolution is driven by the cross-over of protonated species or oxidation products from the cathode. This mechanism provides a rational explanation for the observation that H_2 evolution is significantly enhanced under high-voltage and high-temperature conditions even without increased water content. Furthermore, trace water exacerbates the corrosion of conductive carbon black, accompanied by the generation of CO_2 and CO. Relevant reaction equations are shown in R28–R29.

2.2.3. Complex interaction mechanisms driven by electrode crosstalk

Electrode crosstalk, defined as the diffusion of byproducts generated at one electrode to the counter electrode, serves as a critical source of gas production [122]. Such interactions accelerate capacity degradation

by altering SEI growth and promoting further reductive side reactions at the anode [123]. Consequently, a comprehensive understanding of the interactions between the cathode and anode remains important for improving battery lifetime.

Transition metal dissolution and migration represent a primary mechanism of crosstalk in LIBs. Transition metals can dissolve from the cathode, often facilitated by HF or other acidic species in the electrolyte, migrate through the electrolyte, and subsequently deposit on the anode. [124,125]. Solchenbach et al. [109] utilized OEMS to investigate the impact of Mn^{2+} and Ni^{2+} on graphite anodes with pre-formed SEI layers in the transition-metal-free electrolyte. Their findings revealed that while the catalytic activity of nickel ions is effectively suppressed by the SEI, Mn^{2+} can penetrate the SEI layer via ion exchange and reach the graphite surface. The reduction of Mn^{2+} catalyzes the decomposition of LEDC into Li_2CO_3 and C_2H_4 (R30). This process compromises the integrity of the interphase and induces further reduction of fresh electrolyte solvent to generate additional C_2H_4.

The consumption of CO_2 constitutes another significant reaction within the crosstalk mechanism. Ellis et al. [34] injected various gases into pouch batteries and analyzed the evolution using Archimedes' principle and GC to elucidate the gas evolution behavior. Their results demonstrated that CO_2 is the most rapidly consumed species and becomes depleted after 100-hour storage. Furthermore, Sloop et al. [126] proposed a shuttle mechanism involving CO_2. CO_2 generated at the cathode diffuses to the anode and undergoes reduction to form lithium oxalate. The solubility of lithium oxalate allows it to migrate back to the cathode for re-oxidation to CO_2 as shown in R31–R32. While this cyclic process drives reversible self-discharge, the concurrent irreversible reduction of CO_2 to carbonates permanently reduces capacity, and the continuous consumption of CO_2 triggers further electrolyte polymerization, ultimately leading to severe power fade.

Oxygen crosstalk plays a critical role in battery aging particularly for nickel-rich cathodes under high-voltage cycling [127]. During long-term cycling, layered cathode surfaces progressively undergo severe reconstruction from the layered structure to disordered spinel/rock-salt phases [128–130]. This structural degradation is accompanied by lattice oxygen evolution under high cut-off voltage cycling, especially for Ni-rich cathodes at deeply charged states [131]. The oxygen released from the cathode further drives cathode-to-anode cross-talk, and the resulting oxygen-derived electrolyte decomposition products are subsequently consumed at the graphite/SEI interface in NMC/graphite full batteries [110,127]. These parasitic reactions continuously deplete the active lithium inventory by promoting further SEI growth and interphase thickening at the graphite anode [109,123,132].

3. The path-dependent influence of aging on TR characteristics

The gas-evolution mechanisms summarized above also determine how aged batteries respond during heating or abuse. By changing the internal reaction environment, they affect heat release, pressure buildup, and the onset of self-heating [133]. Section 3 therefore connects these microscopic reactions with macroscopic thermal safety indicators. Local interfacial degradation, such as SEI dissolution, lithium plating, and cathode oxygen release, changes both gas generation and heat release, which can shift the thermal safety limits of LIBs. TR in LIBs manifests as a cascading sequence of uncontrolled exothermic reactions initiated under abusive operational conditions. As depicted in Fig. 5, this phenomenon can be quantitatively defined through three distinct temperature parameters: the onset temperature for self-heating initiation (T_1), the critical temperature for TR activation (T_2), and the peak temperature achieved during the thermal event (T_3) [134].

Specifically, T_1 corresponds to the onset of early exothermic reactions, which are commonly associated with the thermal decomposition of metastable SEI components. This stage is accompanied by heat release and the evolution of gases such as C_2H_4 and CO_2, as schematically represented in Table 2 (reactions R33–R35) [135]. It is worth noting that

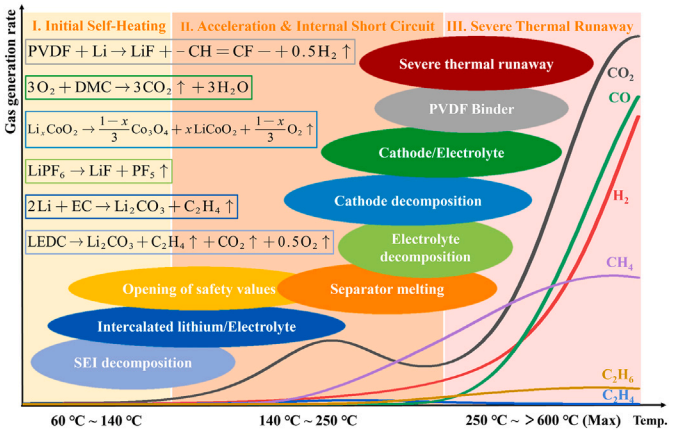

Fig. 5. The temporal sequence of gas evolution during the TR process of LIBs.

the formulation for LEDC decomposition (R34) serves as a schematic representation of a global process, which inherently involves multiple concurrent pathways and complex products. As heat accumulation intensifies, the separator progressively loses its structural integrity, and an ISC is triggered at T_2. The battery then rapidly enters the final stage of TR, driven by the combined effects of cathode oxygen release, exothermic reactions between the cathode, anode, and electrolyte, and the instantaneous heat release associated with ISC (R36–R45) [136]. The resulting massive energy release drives the battery temperature toward its peak value, T_3, and markedly elevates the risks of fire and explosion. Therefore, T_1, T_2, and T_3 are not fixed values but vary with the specific aging pathway. The following sections discuss how high-temperature aging, low-temperature aging, high-rate cycling, and overcharge/over-discharge modify the internal side reactions and reshape TR behaviors and thermal safety boundaries.

3.1. Impact of high-temperature aging on TR behaviors

High-temperature operation represents a critical challenge for electrochemical energy storage systems deployed across diverse applications, from electric vehicles to large-scale grid storage and harsh-environment electronics [146]. Sources of thermal stress include hot environmental exposure [41], improper charging protocols [147], and prolonged high-load cycling [148]. These conditions kinetically accelerate interfacial parasitic reactions and precipitate internal structural

Table 2
Gas generation reactions of LIBs during TR process.

Reaction	No.	Ref.
Decomposition and regeneration of SEI		
$(CH_2OCO_2Li)_2 \rightarrow Li_2CO_3 + C_2H_4 + CO_2 + \frac{1}{2}O_2$	R33	[137]
$LEDC \rightarrow Li_2CO_3 + C_2H_4 + CO + CH_3CH_2CO_2Li$	R34	[138]
$2Li + (CH_2OCO_2Li)_2 \rightarrow 2Li_2CO_3 + C_2H_4$	R35	[139]
Anode reacts with electrolyte		
$2Li + EC \rightarrow Li_2CO_3 + C_2H_4$	R36	[140]
$2Li + DMC \rightarrow Li_2CO_3 + C_2H_6$	R37	[140]
Decomposition of electrolyte		
$DMC + PF_5 \rightarrow CH_3OCOOPF_4 + CH_3F$	R38	[141]
$\frac{5}{2}O_2 + EC \rightarrow 3CO_2 + 2H_2O$	R39	[142]
$3O_2 + DMC \rightarrow 3CO_2 + 3H_2O$	R40	[142]
$O_2 + EC \rightarrow 3CO + 2H_2O$	R41	[142]
$\frac{3}{2}O_2 + DMC \rightarrow 3CO + 3H_2O$	R42	[142]
Binder reacts with anode		
$PVDF + Li \rightarrow LiF + -CH{=}CF- + \frac{1}{2}H_2$	R43	[143]
$CMC{-}OH + Li \rightarrow CMC{-}OLi + \frac{1}{2}H_2$	R44	[144]
$2Li + (-CH_2CF_2-) \rightarrow 2LiF + (-CH=CH-)_{residue}$	R45	[145]

deterioration [149]. Key degradation mechanisms include transition metal dissolution and particle rupture at the cathode, alongside continuous SEI decomposition and regeneration at the anode [150,151]. These irreversible processes extend beyond capacity loss to fundamentally alter the safety characteristics of the battery. Specifically, high-temperature aging can shift different thermal-safety metrics in different directions, including T_1, T_2, the interval between T_1 and T_2, self-heating rate, and, in some cases, T_3 and peak heating rate [152]. Accordingly, this section discusses high-temperature aging through specific safety metrics rather than treating it as a monotonic increase in hazard severity.

Previous studies demonstrate that the effects of high-temperature aging on thermal performance are regime-dependent, with distinct mechanisms dominating at different temperature intervals [153]. As depicted in Fig. 6(a), under mild thermal stress (typically below 45 °C), the anode undergoes minimal morphological changes aside from slight SEI thickening [154], and TR characteristics remain comparable to fresh batteries [155]. However, within the 25–45 °C range, the time interval between T_1 and T_2 narrows progressively [154]. This acceleration is closely associated with the compositional and structural evolution of the SEI layer. Specifically, thermally unstable organic components (e.g., $(CH_2OCO_2Li)_2$) gradually convert into stable inorganic species (e.g., LiF, Li_2CO_3) [85], leading to a porous and less cohesive SEI morphology. The increased surface area facilitates faster exothermic reactions with the electrolyte, thereby accelerating heat accumulation and reducing the response window before TR occurs. Therefore, while no severe degradation is observed, the narrowing of the TR initiation window warrants attention even during mild thermal aging.

Under conditions of moderate thermal stress, the SEI layer tends to evolve into a thermally resilient barrier that effectively delays the onset of TR or T_1 [156]. For instance, Börner et al. [19] reported that cycling at 45 °C facilitates the formation of a protective SEI and elevates T_1, thereby enhancing battery safety (Fig. 6(b)). This trend was statistically corroborated by Garcia et al. [157], where batteries aged at 50 °C exhibited a substantial 17 °C increase in T_1 compared to fresh batteries. Further thermal analysis by Ren et al. [134] using differential scanning calorimetry (DSC) confirmed these benefits. As shown in Fig. 6(c), the exothermic peak typical of fresh anodes vanished after storage at 55 °C, accompanied by a significant reduction in total heat release from 2599.9 to 2084.9 J/g.

To elucidate the underlying causes, Zhang et al. [158] utilized accelerating rate calorimetry (ARC) and observed that high-temperature calendar aging not only raised T_1 but also suppressed self-heating rates. While this study focused on macroscopic thermal behaviors, Liu et al. [159] provided mechanistic insights by identifying SEI thickening as the primary driver. As illustrated in Fig. 6(d), the thickened SEI serves as a physical barrier that isolates the lithiated anode from the electrolyte and retards exothermic interfacial reactions. It is important to distinguish that cycling aging introduces dynamic degradation factors like gas evolution and mechanical fatigue, which are less prominent in static calendar aging analyzed by Ren et al. [134]. Consequently, disentangling these static and dynamic mechanisms is crucial for a precise understanding of how elevated temperatures reshape the safety limits of LIBs.

Under conditions of severe thermal stress (e.g., ~60 °C), the SEI undergoes concurrent decomposition and regeneration, with the latter initially dominating [154,160,161]. However, the regenerated SEI is structurally loose, implying a larger specific surface area and increased reactivity. Lithium plating also frequently occurs on the anode surface [162]. These side reactions intensify exothermic behavior and lower the barrier for TR initiation [163]. Consequently, the main manifestation of safety deterioration at this stage is an earlier onset of self-heating and separator shutdown, i.e., lower T_1 and T_2, together with a shorter interval between T_1 and T_2. Zhang et al. [52,164] conducted adiabatic TR and overcharge tests on batteries cyclically aged at 60 °C. Their results revealed that high-temperature cyclic aging reduced both T_1 and T_2. The reduced activation energy associated with the T_1-to-T_2 transition

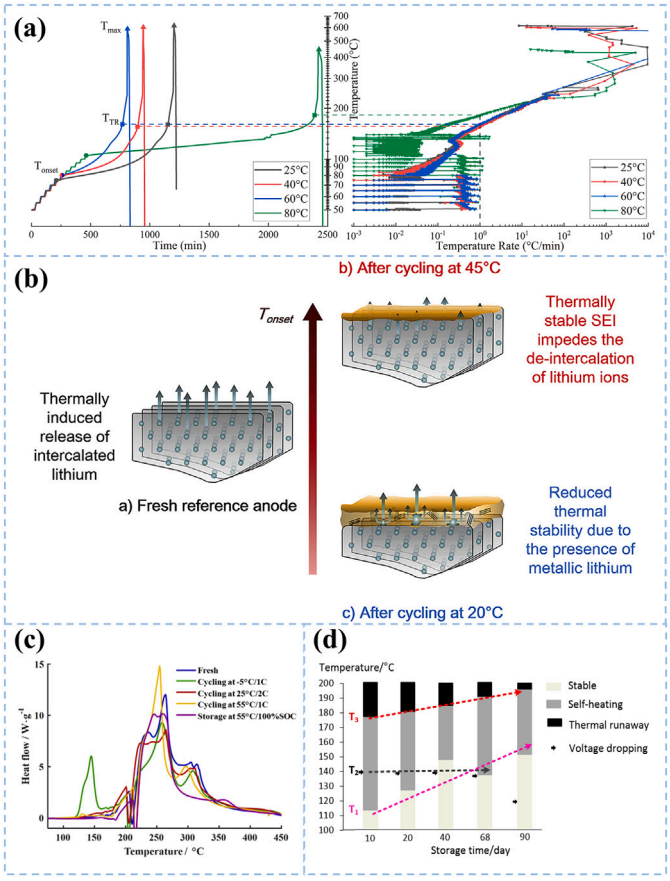

Fig. 6. Thermal characteristics under high-temperature aging: (a) TR behaviors of LIBs after various degrees of high-temperature aging [154]. (b) Changes in the SEI on the anode surfaces after cycling at 20 °C and 45 °C [19]. (c) Heat flow curves under different aging conditions [134]. (d) Temperature changes during TR after storage for different durations [158].

implies that TR is more easily triggered. Moreover, the voltage plateau and peak voltage before TR appear earlier, indicating that severe side reactions have significantly eroded thermal stability. Complementing these findings, Zhang et al. [39] identified that transition metal dissolution and reductive gas attack destabilize the cathode lattice. Both cyclic and calendar aging at 60 °C induce progressive reductions in T_1 and T_2 by 20–30 °C. The generated gas ruptures the aluminum-laminated layer and accelerates electrolyte evaporation. This loss of active materials and electrolyte limits the reactant inventory available for runaway reactions. Consequently, the total heat release is capped, leading to a decrease in maximum temperature (T_3) and peak heating rate, which can reduce the ultimate event severity [133].

At elevated temperatures (e.g., ≥80 °C), although spontaneous TR is not yet triggered, the protective function of the SEI becomes severely compromised. Degradation turns irreversible as decomposition outpaces regeneration [154]. Rather than immediate TR, the dominant outcome at this stage is extensive SEI collapse and sustained depletion of active lithium. Once the anode becomes fully exposed, it exhibits heightened sensitivity to subsequent thermal or mechanical abuse, implying that the energy barrier for initiating exothermic reactions is significantly reduced [165]. Chu et al. [166] systematically investigated the effects of cycling at 80 °C on thermal safety after 200 cycles at 1 C. Post-mortem analysis revealed that the accumulation of organic decomposition products such as $ROCO_2Li$ markedly impaired thermal stability and accelerated early-stage TR reactions. Specifically, aged batteries exhibited an approximately 10% higher heat release rate in the early stage

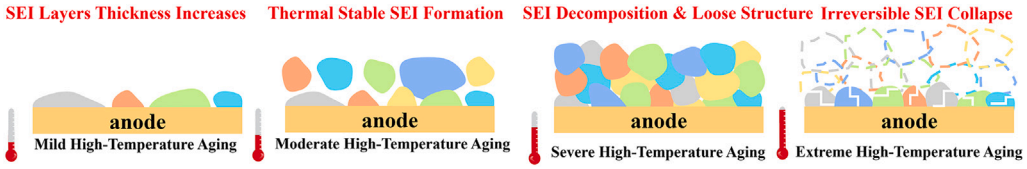

Fig. 7. Impacts of high-temperature aging on SEI layers with different aging degrees.

of TR, whereas the final event severity remained constrained by prior depletion of active materials and electrolyte [167].

In addition to influencing temperature thresholds, high-temperature aging also alters gas evolution behavior during TR [168,169]. Gao et al. [154] reported that pouch batteries aged at 80 °C undergo extensive SEI decomposition, resulting in substantial gas accumulation even prior to TR. The increased internal pressure ruptured the packaging and accelerated electrolyte evaporation, ultimately reducing T_3 and increasing ignition risks. Further insights were provided by Guo et al. [170], who systematically examined gas-phase changes in batteries subjected to high-temperature calendar aging. They found that even under low SOC conditions (0–20%), aging significantly altered TR gas composition and flammability. For instance, the venting gas profile of 0% SOC batteries shifted from a CO_2-dominant profile (85%) to a flammable CO-rich mixture (56%) after aging at 60 °C. Aged batteries exhibited elevated internal pressures and a CO-rich vent-gas mixture, particularly at low SOC. At higher SOC levels (e.g., 70%), severe electrochemical degradation resulted in even higher T_3 values and internal pressures. These results mainly indicate a shift in vent-gas composition after high-temperature aging. The increased CO fraction is important because CO is both flammable and toxic, which may increase the hazard of vented gas exposure and ignition after release.

In summary, the impacts of high-temperature aging on TR behaviors are clearly temperature-dependent, as illustrated in Fig. 7. At mild aging levels, SEI evolution occurs with minimal safety compromise. However, severe or prolonged thermal conditions (>60 °C) promote lithium plating, gas accumulation, and reactive interfacial degradation, collectively reducing TR thresholds and increasing the flammability or toxicity risk of vented gases. These insights highlight the necessity of avoiding extended exposure to high temperatures during storage or operation.

3.2. Impact of low-temperature aging on TR behaviors

Distinct from the material decomposition observed at high temperatures, low-temperature aging compromises safety primarily through the kinetic deposition of metallic lithium. Driven by sluggish ion transport and increased charge-transfer resistance, the anode potential rapidly drops below 0 V vs. Li/Li^+ and precipitates lithium plating [171]. This morphological shift from stable intercalated lithium to thermodynamically unstable metallic lithium fundamentally alters the thermal reactivity profile of the battery [172]. Specifically, deposited lithium can appear as high-surface-area mossy lithium and is associated with reduced thermal stability and earlier exothermic onset [19]. Upon heating, these active deposits react violently with the electrolyte at much lower temperatures than the anode intercalation compound [173]. Consequently, the presence of plated lithium lowers T_1 and intensifies the rate of exothermic reactions, thereby drastically reducing the safety margins of LIBs.

Recent studies have provided extensive experimental evidence supporting the mechanistic understanding above. Wang et al. [18] observed that cycling batteries at −10 °C and 1 C led to the formation of dendritic lithium and electrochemically inactive dead lithium. This morphological degradation was associated with lowered T_1 and T_2 in ARC tests and indicated a higher risk of TR. Ouyang et al. [174] further demonstrated that low-temperature cycling at 0 °C and 1 C until 90% and 80% SOH caused an earlier onset of TR and higher self-heating rates in ARC tests. DSC revealed increased cathode heat release after cycling while ARC tests showed an earlier onset of TR with increased self-heating rates, suggesting that metallic lithium deposits and unstable SEI growth critically deteriorate thermal safety. Postmortem analysis additionally revealed thicker SEI layers and structural degradation of the graphite anode implying LLI and active material loss. In a complementary study, Ren et al. [134] identified a novel exothermic peak in the DSC curve during cycling at −5 °C and 1 C to 80% SOH, which was attributed to reactions between metallic lithium and the electrolyte. The additional heat release led to substantial decreases in T_1, T_2, and the time to TR while T_3 remained nearly unchanged, further emphasizing the role of lithium plating in accelerating TR at low temperatures. Similarly, Friesen et al. [175] reported that low-temperature aging at 0 °C resulted in the accumulation of high surface area lithium (HSAL), which significantly increased reactivity with the electrolyte and led to substantial heat release and the evolution of volatile compounds. Later, they demonstrated that employing an Al_2O_3 coating on the anode surface effectively suppresses the formation of HSAL and enhances thermal safety even in scenarios involving lithium deposition and separator failure [176]. Additionally, Waldmann et al. [155] found that metallic lithium could re-intercalate into the graphite anode during resting periods after low-temperature aging, which helped recover thermal safety similar to fresh batteries as observed in subsequent ARC tests. Conversely, Wu et al. [177] showed that under aggressive conditions at −10 °C and 2 C the self-heating became more intense with declining SOH from 95% to 80%. Interestingly, T_1 and T_2 remained almost unchanged. This phenomenon is likely driven by the synergy between accelerated degradation kinetics under high C-rates and the intrinsic thermal instability of the LCO cathode.

Waldmann et al. [155] further demonstrated that even at a moderate charge rate of 0.5 C, batteries aged at 0 °C exhibited earlier self-heating and higher self-heating rates, indicating severe thermal degradation. Notably, their work emphasized that this decline in thermal safety was primarily driven by exothermic chemical reactions between metallic lithium and the electrolyte rather than ISC caused by dendrite penetration. This conclusion was corroborated by Cai et al. [178] who found no evidence of voltage decay or micro-shorting during low-temperature cycling despite extensive lithium plating. Moreover, under quasi-adiabatic conditions, the heat accumulation further accelerates the temperature rise. Waldmann et al. [155] also noted that metallic lithium becomes molten above 180.5 °C, which increases its interfacial contact area with the electrolyte and further intensifies thermal reactivity.

In addition to thermal characteristics, TR gas evolution behaviors have become an essential factor in assessing battery safety after low-temperature aging. With increasing aging severity, the impact of degradation on gas evolution during TR becomes more pronounced [179]. Under 0 °C and 1 C cycling to various SOH levels, it was observed that in the SOH range between 80% and 100% the decline in anode electrochemical performance and the suppression of lithium plating reactions led to relatively stable internal conditions, resulting in lower gas generation compared to fresh batteries. However, when SOH dropped below 80%, thermal stability declined progressively with earlier safety valve activation at lower triggering temperatures. At SOH 70%, gas release peaked, the safety valve opened at a lower triggering temperature, and the interval between venting and TR became shorter, indicating

a markedly reduced warning window before failure [179]. Moreover, hydrogen gas volume decreases with aging while the amounts of CO, CO_2, and hydrocarbon gases increase. This shift indicates a transition in decomposition mechanisms and may contribute to a reduced risk of secondary deflagration. At 60% SOH, severe structural fracturing of the cathode has been observed. The release of accumulated gas and electrolyte vapor upon venting accelerates thermal reactions and substantially reduces the time between safety valve opening and TR [12]. However, under lower current rates, a significant decrease in solvent vapor, CO_2, and C_2H_4 levels has been observed which may be consumed during the aging process [180]. Ng et al. [48] further showed that low-temperature-aged batteries can follow distinct hazardous pathways depending on the post-aging conditions. After repetitive cycling at −29 °C, compromised batteries left under ambient storage for approximately two weeks underwent catastrophic TR characterized by fire, explosion, and the release of harmful gases. In contrast, similar batteries recovered to room temperature and then cycled exhibited a non-TR failure mode dominated by overpressurized venting, voltage drop, and the release of gases such as CO_2, CO, CH_4, and C_2H_2, but without ignition. These results indicate that low-temperature lithium plating/corrosion may not immediately trigger TR, yet it can markedly reduce the thermal safety margin and create substantial latent hazards.

3.3. Impact of high cycling rates on TR behaviors

The escalating demand for fast-charging capabilities in applications such as unmanned aircraft systems and emergency power supplies necessitates a rigorous understanding of rate-dependent thermal risks [181,182]. Research focusing on the correlation between current density and TR characteristics has thus become imperative [183–185]. Distinct from the time-accumulated passivation observed under low-rate conditions, high-rate cycling shifts the degradation trajectory toward a fracture-dominated regime driven by mechanical stress and kinetic polarization [186]. This aggressive operating mode triggers particle microcracking and lithium plating which expose highly reactive fresh surfaces to the electrolyte [187]. Consequently, these structural and chemical instabilities significantly lower the TR thresholds and accelerate the heat generation rates during failure events.

High current densities during fast charging exacerbate side reactions, posing a significant challenge to both battery performance and thermal safety [188–190]. A key degradation mechanism is the severe polarization effect at high rates, where the lithium-ion migration rate to the anode surface outpaces its intercalation into the graphite layers [27]. This leads to undesired lithium-ion accumulation at the anode surface rather than intercalation [191]. Consequently, the electrode potential falls below the Li/Li^+ redox potential, promoting lithium-ion reduction to metallic lithium deposition on the anode surface [192]. Lithium plating facilitates side reactions with the electrolyte, ultimately degrading thermal stability [193,194]. Meanwhile, rapid lithium-ion transport induces significant volumetric changes and mechanical stresses, causing particle cracking and secondary fractures in both anode and cathode active materials [195]. At the cathode, high-rate cycling can elevate the operating voltage, triggering irreversible phase transitions from layered to spinel and eventually to rock-salt structures [196,197]. The structural deterioration compromises the kinetics of lithium-ion transport and lowers the overall safety threshold of batteries [198]. In addition, high-rate cycling significantly elevates the internal temperature due to Joule heating and exothermic side reactions. This elevated temperature accelerates electrolyte decomposition and gas generation [199], which not only obstructs lithium-ion transport but also poses a potential fire hazard due to the electrolyte being flammable [200].

Experimental studies have provided compelling evidence for these degradation mechanisms. For example, Ouyang et al. [184] investigated the aging and thermal behavior of NCM523 18,650 batteries cycled at various rates (1 C, 2 C, and 4 C). Their results revealed a clear acceleration of capacity degradation with increasing cycling rates as shown in Fig. 8(a). DSC curves of aged electrodes showed greater heat release, indicating more severe exothermic side reactions attributable to increased lithium plating and electrolyte decomposition [201]. Consistently, aged batteries exhibited worsened thermal behaviors during heater-induced TR, characterized by an earlier onset of ignition and TR [183], a lower T_2 and a higher temperature rise rate [202]. These findings indicate that higher cycling rates generally make TR easier to trigger and accelerate early-stage heating, but they do not support a universal monotonic increase in final TR severity.

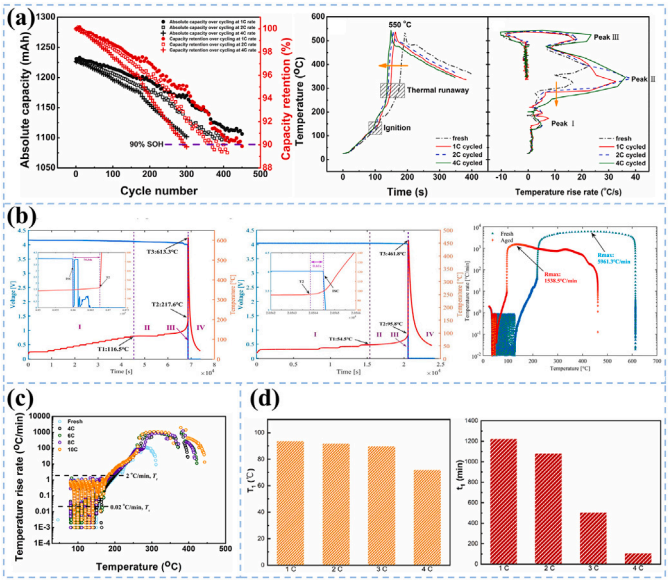

Fig. 8. Thermal characteristics of aged LIBs with high cycling rates: (a) the capacity degradation and temperature characteristics during TR of the batteries cycled with various rates [184]. (b) Comparison of ARC results and the relationship between temperature and temperature rise rate for aged and fresh batteries [185]. (c) The temperature rise rate during TR for fresh batteries and aged batteries with various cycling rates [203]. (d) Key parameters during TR at 50% SOC with different cycling rates [202].

The impact on T_3, however, presents a more nuanced picture. While some studies, such as Ouyang et al. [184], found no significant difference in T_3 between aged and fresh batteries (Fig. 8(a)), attributing this to reduced mass ejection during the rapid TR event [199], others have reported notable changes in T_3 with increased cycling rates [183,202–204]. For instance, Huang et al. [183] investigated the impact of high-rate cycling on TR propagation. Their results revealed that increasing the number of charge/discharge cycles (30, 50, 100 cycles) at 3 C cycling rates significantly accelerates TR initiation, with the TR onset time t_1 advancing by 317 s and T_3 decreasing by 17.2%. Fragments of active material particles and increasing fibrous impurity deposition on the particle surfaces after high-rate cycling suggest a lower battery safety threshold [205]. Moreover, the decreased T_3 and maximum temperature rise rates are found under higher cycling rates [204] or lower SOH [185]. The decline in T_3 and maximum temperature rise rates at high cycling rates in Fig. 8(b) has been attributed to reduced active materials involved in exothermic reactions, owing to the loss of active materials and the depletion of electrolytes, resulting in reduced heat release [206]. On the contrary, Ouyang et al. [203] studied the degradation and thermal safety of aged batteries cycled at 4 C, 6 C, 8 C, and 10 C to 90% SOH, respectively. They observed higher T_3 and faster temperature rise rates of aged batteries, with exacerbated thermal risks as the cycling rate increases (Fig. 8(c)). This is primarily attributed to the lithium plating on the anode surface [207]. These seemingly contradictory observations can be reconciled by considering the specific test conditions. A comprehensive study by Huang et al. [202] demonstrated

that TR characteristics are strongly dependent on both the cycling rates and SOC. They conducted experimental studies to investigate the thermal performance of batteries with multiple SOC (50%, 75%, and 100% SOC) and cycling rates (1 C, 2 C, 3 C, and 4 C). Their results showed that, at a given cycling rate, T_1 decreased by 1.2%–12.3% and the time to reach T_1 (t_1) decreased by 28.3%–41.8% under different SOC conditions. Meanwhile, a more severe impact is observed when varying the charge rate. Elevating the cycling rates from 1 C to 4 C causes a substantial decline in thermal stability, with T_1 and t_1 decreasing by 13.5%–23.2% and 78.2%–90.9%, respectively (Fig. 8(d)). Ultimately, battery capacity mainly dictates T_3, as well as the maximum heat release rate and peak mass loss rate, since higher capacity batteries contain a greater mass of electrochemically active materials. This, in turn, is associated with more reactive substances participating in the exothermic reactions and more severe ejection during TR. These findings suggest that the contradictory observations regarding T_3 are likely due to differences in the SOC conditions and capacity under which the TR tests were performed [208].

Although quantitative data on the link between C-rates and TR gas behavior is scarce [209], evidence suggests that high C-rates cause lithium plating and interfacial instability, leading to earlier and more severe TR [210]. Moreover, the resulting rapid reactions tend to produce more CO, increasing the risk of combustion [211].

Taken together, low-temperature cycling and high-rate cycling share a common anode-side feature. Both pathways can induce lithium plating and abnormal SEI evolution, leading to highly reactive metallic lithium on the anode surface. Consequently, both aging modes consistently lower T_1, accelerate early-stage exothermic reactions, and shorten the critical safety warning window. However, substantial differences emerge regarding their driving forces and structural consequences. Low-temperature aging is predominantly driven by sluggish ion transport. Under non-extreme operating conditions, the cathode bulk structure remains relatively intact, meaning TR deterioration is largely dominated by the anode-side lithium inventory. In contrast, high-rate cycling is characterized by severe kinetic polarization coupled with intense Joule heating. This electro-thermomechanical stress not only exacerbates lithium plating but also induces widespread mechanical degradation, including particle micro-cracking and irreversible phase transitions within the cathode. Consequently, high-rate aging profoundly destabilizes the entire battery system, often triggering TR earlier than low-temperature aging. However, because this severe structural damage and elevated internal temperatures concurrently consume massive amounts of active materials and electrolyte during the aging process itself, the ultimate TR severity (e.g., T_3 and peak heating rate) in high-rate aged batteries is heavily constrained by reactant depletion. This limitation explains the highly condition-dependent T_3 trends discussed previously.

3.4. Impact of overcharge and over-discharge on TR behaviors

Battery packs consist of many individual batteries connected in series and/or parallel [212]. Manufacturing tolerances, nonuniform operating conditions, sub-optimal battery management, and inter-module imbalance can drive battery-level overcharge or over-discharge [213]. Sustained overcharge or over-discharge cycling produces pronounced structural and interfacial degradation at both electrodes. In practical energy storage systems, these electrical imbalances may also coexist with mechanical stress, such as continuous vibration, swelling constraints, or local compression. Such mechanical-electrical coupling can aggravate interphase damage by promoting SEI fracture and exposing fresh reactive surfaces to the electrolyte. As a result, coupled stress may alter subsequent gas evolution pathways and TR behaviors compared with purely electrical aging. To understand how these system-level imbalances and coupled stressors lead to catastrophic thermal hazards, it is crucial to clarify the distinct electrochemical degradation mechanisms driven by overcharge and over-discharge conditions.

Under overcharge cycling, the cathode experiences excessive delithiation, decreasing structural stability [214]. Subsequent lattice expansion and oxygen migration trigger irreversible phase transitions (e.g., layered→ spinel/rock-salt), culminating in particle cracking and severe structural damage [215]. In parallel, transition-metal dissolution intensifies, further undermining electrode integrity and interfacial reactivity [216]. At the anode, Li plating forms dendritic protrusions that may pierce the separator [217,218]. Meanwhile, plated Li reacts with the electrolyte, consuming solvent/salt and rebuilding a thick yet fragile SEI that impedes Li^+ transport, raises impedance, and accelerates capacity fade [219,220]. In contrast, under over-discharge cycling, extensive delithiation shifts the anode to more positive potentials (vs. Li/Li^+) [221], thereby driving dissolution of the Cu current collector [222]. Dissolved Cu species migrate and redeposit as metallic dendrites on the separator/cathode, increasing internal short-circuit risk [223]. Corrosion/oxidation of Cu accelerates anode delamination and loss of electronic contact [224]. Electrolyte decomposition releases heat and combustible gases (e.g., CO, H_2, C_2H_4) [214], raising internal pressure and feeding combustion or even explosion at elevated temperatures, thereby precipitating TR [225].

These aging mechanisms reduce the thermal stability of LIBs [226]. Different TR triggers should also be distinguished because the gas-generation pathway depends on how TR is initiated. External heating mainly drives SEI decomposition and subsequent bulk reactions. In contrast, overcharge continuously supplies electrical energy, leading to strong cathode delithiation and lithium plating at the anode. The resulting reactive internal environment can increase Joule heating, accelerate reactions involving freshly plated lithium, and change the apparent gas-evolution sequence compared with externally heated batteries. Xie et al. [227] investigated NCM523 18,650 batteries (normal operation: 2.75-4.2 V) subjected to overcharge cycles up to 4.8 V. TR triggered by heating occurred earlier and the T_2 decreased as presented in Fig. 9(a), suggesting reduced thermal stability due to lithium plating, the formation of unstable SEI layers, and the consumption of electrolyte [228]. Combustion intensity during TR also increased, amplifying thermal hazards [229]. To extend these observations across a wider range of overcharge severity, Zhang et al. [230] comprehensively investigated the thermal behaviors of batteries with different degrees of overcharge. As can be seen from Fig. 9(b), critical TR temperatures, especially T_1, decreased monotonically with the degree of overcharge, in line with increasing Li plating. Furthermore, T_3 displayed a decreasing trend in batteries experiencing more severe overcharging conditions. This negative correlation stems directly from the progressive depletion of internal reactants during overcharge. Notably, irreversible side reactions, including electrolyte decomposition and its interaction with deposited lithium metal, persistently deplete the electrolyte. The resulting loss of these critical components significantly diminishes the battery's total stored energy available for release during TR, consequently suppressing T_3. Similarly, Yang et al. [231] studied lithium iron phosphate (LFP) batteries after overcharge cycling. T_1 dropped markedly at a 4.5 V cutoff attributed to SEI thickening, but changed little at 3.65/4.0/4.2 V as depicted in Fig. 9(c). Huang et al. [232] revealed that the major damage induced by slight overcharge cycles was LLI, LAM, and conductivity loss (CL), and the LLI damage appeared first [233], followed by the LAM and CL [234]. Taken together, these results indicate that batteries exhibit a certain tolerance to slight overcharging [232,234]. However, Zhang et al. [235] pushed the overcharge cutoff to 5.0 V to probe accelerated aging. Early-stage heat was dominated by severe side reactions inside the battery. Electrolyte oxidation and Li deposition were the two major early-stage heat sources [236]. Importantly, tolerance to further overcharge decreased as degradation progressed. By contrast, at higher charging voltages, elevated temperature mitigated Li plating, particle cracking, and SEI formation, partially relieving degradation [237,238]. To resolve TR characteristics versus SOH (100%, 90% and 80%), Feng et al. [239] overcharged batteries to 4.5 V and measured thermal responses. T_2 remained approximately 103 °C across SOH, suggesting minimal changes in separator shutdown behavior [240]. Nonetheless, other studies reported an increased thermal-shrinkage rate of aged

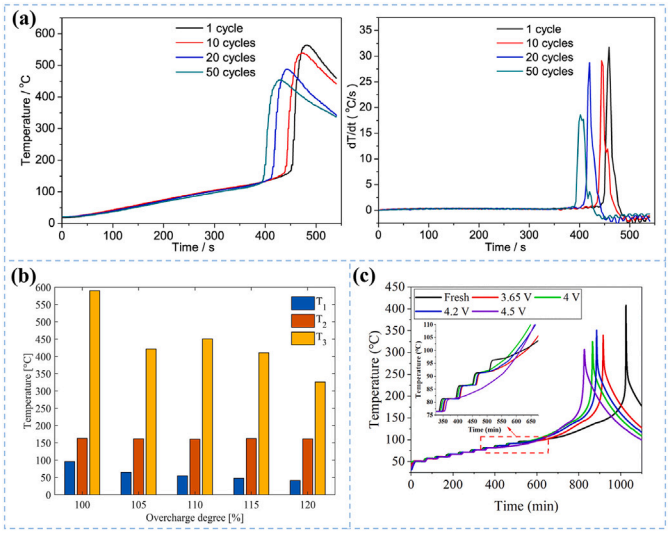

Fig. 9. Thermal characteristics under overcharge aging: (a) TR surface temperature and temperature rise rate of the batteries with different overcharge cycles [227]. (b) Comparison of the TR temperatures of the aged batteries tested at 100% SOC after corresponding overcharge aging [230]. (c) The ARC test results of LFP batteries before and after aging at various voltages [231].

separators, potentially elevating internal-short risk [215,216,219,241]. With deeper overcharge, TR occurred earlier, and a voltage-curve inflection can serve as an early warning signal. For the influence of overcharge aging on T_3, different scholars have proposed different perspectives. Many studies show T_3 decreases after overcharge cycling, attributed to reduced stored energy and electrolyte depletion [218,231,238,240,242]. However, some studies have also reported that T_3 can increase as overcharge aging becomes more severe [214]. Therefore, further research is needed to clarify the effect of overcharge cycling aging on T_3.

For the impacts of overcharge, it is crucial to note that over-discharge aging likewise has profound impacts on thermal safety [243]. Yang et al. [244] investigated aging and thermal safety versus over-discharge cutoff voltage. Lower cutoff voltages yielded lower T_2, T_3, earlier TR trigger time and peak dT/dt relative to fresh batteries as illustrated in Fig. 10(a). Combustion intensity during TR weakened, indicating reduced thermal hazard. Conductivity loss and LLI are the main aging reasons for batteries discharged to 0.5 V, accounting for 75.92% and 64.88%, respectively. Ouyang et al. [242] likewise cycled 18,650 lithium batteries of the same cathode system to 0.5 V. As is evident in Fig. 10(b), ignition occurred earlier at lower temperatures, the battery mass declined sharply, TR advanced and T_2 decreased, indicating heightened TR risk after long-term over-discharge cycling. Likely contributors include degraded cathode thermal stability. Considering capacity scaling, Ouyang et al. [245] highlighted that batteries with higher nominal capacity were more sensitive to abuse due to stronger polarization/heat generation and poorer lithium/heat distribution. When rate effects are superimposed, Yin et al. [246] coupled high-rate cycling with over-discharge on high nickel batteries. The results highlight that separator shutdown temperature decreased by 22.3 °C, and meltdown time shortened to 1999 s. T_3 remained similar, suggesting comparable TR severity. Post-mortem analysis indicated irreversible damage to active materials, increasing safety risk. Conclusively, under comparable slight abuse, Zhang et al. [240] compared the impact of slight overcharge and slight over-discharge on the thermal safety characteristics of LIBs. At similar minor abuse, T_1 decreased significantly, whereas T_2 and T_3 changed little as shown in Fig. 10(c). Thermal deterioration was greater for slight over-discharge than for slight overcharge. Characterization links Li plating (slight overcharge) and Cu plating (slight over-discharge) to decreased thermal stability, with different severities for the two cases.

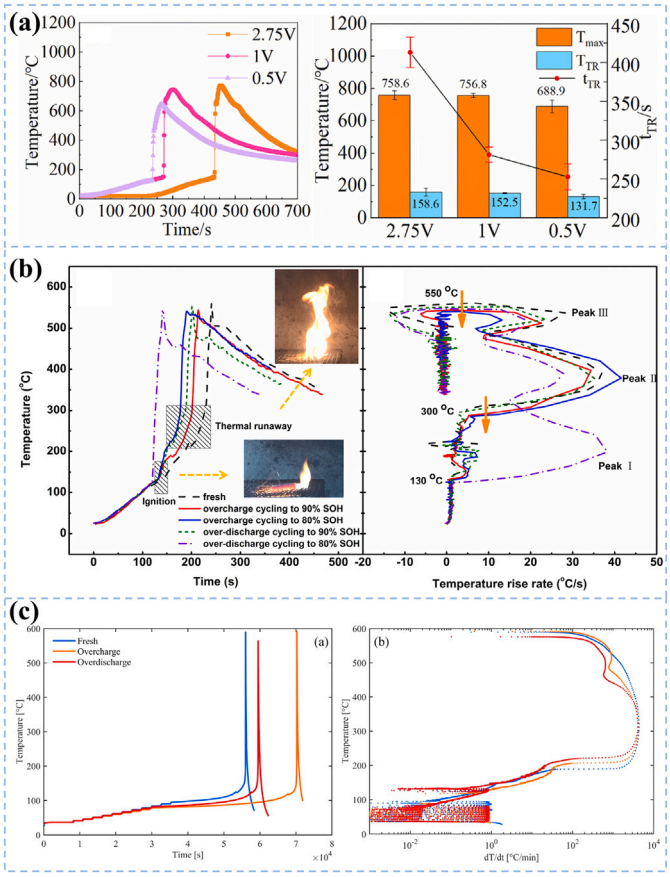

Fig. 10. Thermal characteristics under over-discharge aging: (a) TR surface temperature and TR trigger time of the batteries with different over-discharge cut-off voltages [244]. (b) The surface temperature and surface temperature vs. temperature rise rate curves during TR [242]. (c) Temperature vs time and temperature vs temperature rate curves of tested batteries [240].

In summary, both overcharge and over-discharge induce distinct yet severe degradation pathways, ranging from cathode lattice destabilization and transition metal dissolution to anode Li/Cu plating and SEI growth, which collectively diminish thermal stability and advance TR initiation. Critically, even slight abuses beyond safe voltage windows accumulate irreversible damage, significantly reducing safety margins. To effectively mitigate risks, the foremost engineering priority is for battery management system (BMS) to enforce strict operational voltage control and integrate algorithms for early-fault detection. At the materials level, improved electrolytes and electrode designs should be developed to intrinsically suppress detrimental reactions such as lithium plating and copper dissolution. Furthermore, advancing toward a proactive safety paradigm, systems should employ predictive monitoring that analyzes real-time data to intervene before TR occurs.

4. The crucial role of gaseous species as indicators for LIB aging diagnosis and TR characteristics prediction

In this section, indicator gases are defined as specific gaseous species whose evolution characteristics (e.g., presence, onset temperature, release rate, and cumulative volume) can be linked to particular degradation pathways or the precursor stages of TR. To serve as effective diagnostic and predictive markers, these gases should meet several practical requirements. In this review, the corresponding utility of these gases is evaluated by mechanistic specificity, sensitivity, and robustness across operating conditions [10,247,248].

4.1. Diagnosing specific degradation pathways via characteristic gas signatures

Gaseous species function as sensitive chemical indicators of the internal health of LIBs [10,209]. These indicators offer earlier detection of anomalies compared to traditional voltage and temperature monitoring [247]. The release of specific gases provides direct evidence of interphase instability and electrolyte decomposition [248]. Such chemical signals reflect the degradation history and aging pathways of the battery. Characteristic gas profiles allow for the identification of lithium plating and SEI growth. This mechanistic understanding forms the basis for predicting TR risks in aged batteries [249]. Quantitative gas analysis supports the development of accurate safety assessment models for second-life applications [250].

4.1.1. CO_2: an indicator for SEI/CEI evolution

CO_2 is one of the main components of the evolved gases and serves as a primary chemical indicator for the cumulative degradation of interphase layers and cathode stability [251]. The thickness and chemical composition of the SEI change significantly during the long-term aging process. In fast-charging aged batteries, thickened interphase layers tend to contain higher concentrations of organic metastable species such as LEDC [71]. These components undergo thermal decomposition at relatively low temperatures to release substantial volumes of CO_2 and C_2H_4. Cathode aging also promotes particle cracking and the premature release of lattice oxygen at high SOC [252]. This structural instability accelerates the oxidation of carbonate solvents and increases the generation rate of CO_2 during early thermal failure. Recent studies on aged batteries demonstrate that the onset temperature for gas release shifts downward as the SOH declines [253]. The total volume of CO_2 produced during initial heating provides a quantitative measure of the previous electrolyte decomposition history. Advanced analysis of gas signatures suggests that CO_2 evolution is closely associated with interphase evolution and Li-containing reactions at lithiated anodes [31]. This chemical evidence allows researchers to distinguish between different aging pathways such as transition metal dissolution and interphase thickening. Linking these gas profiles to the degradation state forms the scientific basis for predicting the safety margin of retired batteries in second-life applications.

The fundamental link between degradation history and gas signatures supports the practical implementation of early warning systems. CO_2 is often one of the earliest detectable gases originating from the instability of the SEI and the CEI. It can be detected even before the characteristic T_1 is reached [254]. Fernandes et al. [255] utilized a high-resolution gas detection setup to monitor the temperature and gas generation behavior of LFP batteries during overcharging. Their monitoring system detected large amounts of DMC and CO_2 during the early stages of failure. These findings suggest that the internal temperature remains low while electrolyte vapor and decomposition products begin to accumulate. Once the battery casing ruptures, the gas production rate increases rapidly and produces harmful species such as CH_3OCH_3 and C_2H_4. Using infrared spectroscopy to monitor these CO_2 signals in real time enables active intervention before TR occurs. Cai et al. [254] proposed a generation model to predict gas release based on internal pressure mechanics and utilized a non-dispersive infrared sensor to determine a specific CO_2 concentration alert threshold of 30,000 ppm. Their experimental results demonstrate that gas sensors exhibit a significantly faster response compared to traditional surface temperature monitoring. This rapid detection capability enables the system to identify failure signals before TR propagates to adjacent batteries. Beyond static concentration thresholds, incorporating time-resolved gas features, such as the onset sequence of characteristic gases, real-time concentration changes, and short-time transient response patterns, can further strengthen active safety warning systems [256–258]. Recent studies show that gas-based warning benefits from time-resolved monitoring. Gas-detected stages can be distinguished from later reaction-accelerating stages [259], and real-time gas concentration curves can improve abnormality identification compared with relying on a single static threshold alone [258].

4.1.2. H_2: an indicator for lithium dendrite formation

The reaction between metallic lithium and electrolyte components or binders produces H_2 even before the onset of TR [260]. Accumulated lithium plating significantly reduces the thermal stability of the anode and increases the risk of ISC. Therefore, monitoring H_2 concentrations provides a non-destructive method to quantify the degree of lithium deposition during cyclic aging [261]. This early detection is essential because lithium plating acts as a precursor to severe thermal failure in aged batteries.

Jin et al. [262] investigated the gas evolution sequence of LFP packs under overcharge conditions and identified H_2 as a critical indicator of lithium plating [247]. They proposed a non-invasive early warning methodology capable of sensing micron-scale dendrite growth prior to SEI rupture. The proposed strategy is compatible with commercial battery designs and existing BMS, which supports large-scale use. Experimental validation demonstrated that H_2 sensors triggered the earliest alert with a significant time margin of 639 s prior to smoke emission and 769 s prior to fire occurrence. These results indicate that early intervention triggered by specific H_2 signals can help suppress further dendrite growth and delay the transition to uncontrollable TR before smoke or fire occurs [263]. Furthermore, considering that component aging and varying SOC levels significantly alter gas fingerprints, establishing adaptive warning mechanisms based on specific operational histories remains essential [248].

4.1.3. O_2: an indicator for cathode integrity and thermal acceleration

Oxygen evolution serves as the most direct chemical measure of structural degradation in Ni-rich cathode materials. Throughout prolonged cycling, high-nickel cathodes such as NCM811 and NCA undergo phase transitions from the layered structure to the spinel phase and eventually to the electrochemically inactive rock-salt phase while simultaneously releasing lattice oxygen [79]. This chemical signature quantifies the extent of surface degradation and reflects the dissolution of transition metals within aged batteries. High SOC significantly accelerates this process because the instability of bonds between Ni^{4+} and oxygen ions promotes the departure of lattice oxygen from the cathode framework. Such behavior leads to the thinning of the CEI layer and the subsequent loss of its protective capacity. Oxygen-related signals therefore provide mechanistic evidence of cathode degradation, although direct external detection of molecular O_2 should be interpreted carefully.

More critically, the released oxygen often does not escape the battery as stable molecular O_2. Instead, it can act as a highly reactive internal trigger and be consumed through fast secondary reactions. First, a substantial fraction, particularly in the form of reactive singlet oxygen, readily oxidizes carbonate solvents. This initiates cascading electrolyte decomposition that yields secondary gases such as CO_2 and CO [252]. Second, as recently elucidated by Wang et al. [264], oxygen migrating across the separator reacts directly with the lithiated anode, triggering the highly exothermic lithium oxidation reaction (LOR, $4\,Li + O_2 \longrightarrow 2\,Li_2O$). Because a large fraction of evolved oxygen can be scavenged by these internal parasitic reactions before battery rupture, external gas analyzers may detect only limited molecular O_2 during the early stages of failure [79]. Furthermore, singlet oxygen can drive H_2O_2/H_2O-mediated chemistry, promoting $LiPF_6$ hydrolysis to generate HF, which in turn accelerates transition-metal dissolution and interfacial degradation. Consequently, within aged full batteries, oxygen is more accurately classified as an internal mechanistic driver of cathode destabilization and thermal acceleration, whereas externally vented carbon oxides serve as more practical downstream diagnostic signatures. This dual-consumption picture helps explain why oxygen-driven

degradation is strongly correlated with premature T_1/T_2 reduction and an accelerated transition toward irreversible TR [252,265].

4.1.4. C_2H_4: an indicator for interphase stability and rollover risk

C_2H_4 represents a core marker for the growth and evolution of the SEI film on the anode surface. Reductive decomposition of carbonate solvents such as EC consumes active lithium and generates C_2H_4. Stockhausen et al. [266] utilized high-performance liquid chromatography combined with gas chromatography and showed that the preferential decomposition of EC correlates strongly with C_2H_4 generation during the formation and early cycling stages. This correlation provides a foundation for quantifying the initial loss of lithium. Quantitative analysis of C_2H_4 volume directly maps the loss of the active lithium inventory during the cycling process. This gaseous signature offers a sensitive diagnostic tool for the non-destructive evaluation of resistive layers in aged batteries.

The evolution signal of ethylene provides effective warning of anode interface thermal instability before the battery reaches critical temperatures. Jiang et al. [267] used operando electrochemical mass spectrometry and found a significant surge in hydrocarbon gases, especially C_2H_4, at the end of battery life. This phenomenon is defined as a precursor to rollover degradation. The resurgence of this gas marks dissolution and unstable reconstruction of the initial SEI film, which exposes fresh graphite surfaces and triggers stronger electrolyte decomposition. The rapid increase in ethylene concentration usually appears before severe voltage drops caused by overcharge or thermal abuse, providing an early warning window for BMS. Linking ethylene release characteristics to safety boundaries provides a reliable basis for risk assessment in second-life applications.

4.2. Quantifying the impact of aging mechanisms on thermal safety

Fig. 11 summarizes the framework that links gas-generation mechanisms with degradation pathways and thermal safety evolution [134]. Battery aging changes the internal chemical environment and therefore affects key TR characteristics. To systematically map how specific gaseous emissions reflect these altered safety boundaries, Table 3 maps the key gas indicators to their corresponding aging side reactions and associated thermal safety. A comparative analysis of the gas indicators shows that different gases play different roles in TR evolution. Specifically, CO_2 and C_2H_4 serve as the earliest chemical precursors, emerging alongside interphase instability and early self-heating near T_1 [179]. While CO_2 evolution occurs over a broad temperature range of 60–120 °C, C_2H_4 generation is primarily attributed to SEI degradation initiated at approximately 60–80 °C [9,10]. In contrast, H_2 serves as a highly sensitive indicator of anode-side degradation, especially under lithium plating conditions, and can markedly lower T_1 to approximately 60 °C in severe cases [179]. At higher temperatures, O_2 release from the layered cathode governs the transition toward T_2 (typically 140–175 °C for NCM LIBs) [10]. The released O_2 further accelerates electrolyte oxidation, thereby intensifying the propagation from mild self-heating to severe TR. Overall, CO_2 and C_2H_4 are promising early-warning gas signatures, whereas H_2 is a distinct indicator of lithium-plating-induced depletion of the low-temperature safety margin, and O_2 reflects cathode decomposition and accelerated electrolyte oxidation during more severe TR propagation.

Under kinetic degradation pathways characterized by sluggish ion transport, the evolution of H_2 serves as a useful indicator of lithium plating severity. Since accumulated metallic lithium can react exothermically at lower temperatures than lithiated graphite, the detected H_2 volume can provide a useful indication of lithium-plating severity and the possible reduction in the self-heating onset temperature or T_1 [268].

Regarding thermodynamic instability, elevated concentrations of C_2H_4 and CO_2 act as chemical fingerprints for SEI thickening and regeneration caused by elevated temperatures or prolonged cycling. The accumulation of these gases signals the continuous consumption of the liquid electrolyte inventory. This drying-out effect increases internal impedance and reduces the total enthalpy of combustion but can also accelerate early venting risks due to internal pressure buildup [269].

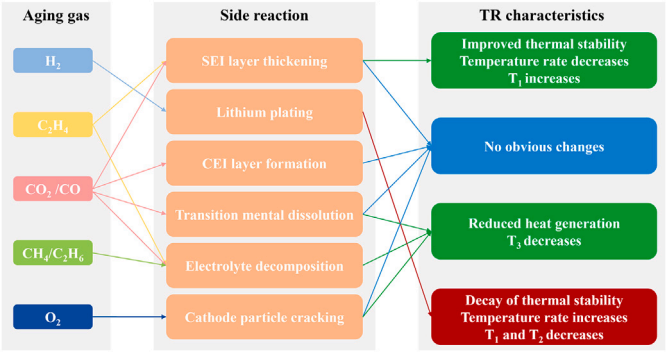

Fig. 11. Schematic illustration of the interplay among gas generation, degradation mechanisms, and thermal safety evolution in aged LIBs [134].

For degradation modes involving structural collapse, such as overcharge or high-voltage cycling, particle cracking facilitates the release of lattice oxygen. As a potent oxidant, this released O_2 accelerates electrolyte combustion kinetics and shifts the separator melting threshold or T_2 to lower values. Consequently, oxygen-related reactions provide a diagnostic link to cathode phase transitions and faster heat release during severe TR propagation [142].

Furthermore, the complex interaction mechanisms driven by electrode crosstalk can be quantified through gas composition ratios. The migration of transition metals correlates with specific CO_2 evolution patterns on the anode side, offering a non-destructive method to assess ISC risks before TR is triggered [152].

Therefore, integrating these characteristic gas indicators enables the establishment of a multi-dimensional safety assessment framework. By correlating gas compositions with specific aging mechanisms, it becomes feasible to quantitatively evaluate the remaining safety margins of aged LIBs. Ultimately, inferring aging pathways and mechanisms from gas evolution characteristics provides a useful basis for predicting TR risks.

4.3. Machine learning-based TR characteristics assessment considering gas evolution behaviors

The progressive degradation of LIBs involves highly coupled electrochemical, thermal, and transport processes. Gas evolution is attractive for safety assessment because it provides more direct chemical evidence of interface instability than voltage or surface temperature alone [254,255]. Nevertheless, the relationship between multicomponent gas signals and macroscopic safety outcomes is strongly nonlinear, path-dependent, and influenced by sensor placement, venting conditions, and operating history. To effectively map these complex relationships, recent studies have increasingly integrated battery safety with machine learning [5]. These data-driven frameworks generally fall into four methodological categories: feature-based machine learning, time-series learning, anomaly detection, and physics-informed machine learning, as summarized in Table 4.

The following paragraphs discuss how each category can contribute to gas-evolution-based TR risk assessment. Feature-based machine learning represents the most direct route for connecting measurable battery responses with safety states, where characteristic variables are first extracted from experimental or operational data and then used as inputs for classification or regression models. These variables may include electrochemical features, thermal features, statistical descriptors, or gas-evolution descriptors, depending on the available sensing platform. For example, a feature-based supervised model using decision trees and support vector machines was reported to classify batteries into

Table 3
Key gaseous species as mechanistic indicators of aging and thermal risk.

Gas	Primary Source Reaction	Aging Pathway	Thermal Safety
CO_2	Li_2CO_3 decomposition (R5, R7) Electrolyte oxidation (R10, R39) LEDC decomposition (R33, R34)	CEI instability Early TR precursor	Cathode stability degradation Early chemical indicator Consumption implies active Li plating Commonly appears near T_1, typically ~60–120 °C [9,10,179]
C_2H_4	EC reduction (R16, R36) LEDC decomposition (R33) Mn^{2+} catalyzed reduction (R30)	SEI regeneration Li plating	Anode side reactions SEI instability/regeneration Major flammable component in TR Linked to SEI degradation starting at ~60–80 °C [9]
H_2	H_2O reduction (R18) Acid/Binder reduction (R27, R43) LiOH conversion (R9)	Low-temp cycling High-rate cycling	Early Li plating marker Trace water/proton shuttle Major flammable component Severe Li plating can lower self-heating onset to ~60 °C Massive binder-related reaction occurs above ~230 °C [12,179,270]
O_2	Lattice oxygen release from layered oxides (R2, R3)	High SOC storage Overcharge	Cathode decomposition Drives electrolyte oxidation In NCM-class batteries, cathode-triggered T_2 is typically ~140–175 °C LFP batteries do not readily release oxygen and show higher TR onset, ~190–220 °C High delithiation (>80% SOC) accelerates oxygen-driven oxidation [10,110,271]

Table 4
Representative machine learning methods for TR risk assessment.

Category	Representative algorithms	Key characteristics
Feature-based machine learning	Support vector machine (SVM); decision tree; random forest; extreme gradient boosting (XGBoost); Gaussian process regression (GPR)	Interpretable features; suitable for limited datasets; dependent on feature selection.
Time-series learning	Recurrent neural network (RNN); long short-term memory (LSTM); gated recurrent unit (GRU); temporal convolutional network (TCN); Transformer	Captures temporal evolution; suitable for early warning; requires time-resolved data.
Anomaly detection	Principal component analysis (PCA); K-means; density-based spatial clustering of applications with noise (DBSCAN); isolation forest; autoencoder	Useful with scarce labels; detects outliers or abnormal patterns; limited physical interpretability.
Physics-informed hybrid learning	Physics-guided machine learning (PGML); physics-informed neural network (PINN); surrogate model; chemical reaction neural network (CRNN); digital twin	Incorporates physical constraints; improves interpretability and generalization; has higher model complexity.

normal batteries, defective batteries, shorted batteries without potential TR, and shorted batteries with potential TR [272]. Random forest has also been used to detect faults after mechanical abuse by extracting features from charge–discharge voltage and current data [273]. Similarly, multiclass relevance vector machine models have been applied to diagnose ISCs. Xie et al. [274] employed a multiclass relevance vector machine (mRVM) model to diagnose ISCs in batteries under mechanical, electrical, and thermal abuse conditions. Four features, including SOC deviation, temperature error, terminal voltage error, and the correlation between charge/discharge current and internal resistance, were extracted to identify hidden internal short-circuit patterns in the continuous space-time domain. The proposed feature-based supervised learning method achieved a grade misjudgment rate of 14.59% and a state misjudgment rate as low as 3.13% across different abuse conditions. Feature-based learning is especially useful when the dataset is relatively small and the extracted features are physically meaningful. Analogous features such as gas onset time, generation rate for different gases, and species ratios are useful when classifying the degradation stage and predicting venting behaviors.

Time-series learning methods are more suitable when the safety-relevant information is contained not only in the magnitude of a signal but also in its temporal evolution. This is important for TR prediction because the transition from early degradation to venting and rapid self-heating is a dynamic process [82,275]. Recurrent neural networks (RNNs), long short-term memory networks (LSTMs), gated recurrent units (GRUs), temporal convolutional networks (TCNs), and Transformer-based models can learn sequential dependencies from multi-sensor histories. In battery prognostics, deep reinforcement

learning has been used for fast-charging control, where the BMS interacts with a battery environment and updates its decisions based on electrochemical and thermal states [276]. Other studies have used time-resolved BMS data, including voltage, current, and temperature, for real-time battery model calibration and health-conscious energy management [277,278]. When gas concentration, temperature, pressure, and voltage are collected as time-series data, such models can identify accelerating degradation trajectories before TR occurs, detect abnormal acceleration in gas generation, correlate gas release with temperature or pressure rise, and predict venting and TR behaviors.

Anomaly detection methods are particularly valuable for TR risk assessment because labeled failure data are usually limited. TR experiments are destructive, costly, and difficult to reproduce, while real-world failure events are rare. Therefore, unsupervised or weakly supervised models can be used to learn the normal behavior of a battery, module, or pack and then identify deviations from this baseline. Principal component analysis (PCA), K-means clustering, DBSCAN, isolation forest, and autoencoder-based models are commonly used for this purpose. PCA-based unsupervised learning has been used for early warning of ISCs by detecting abnormal voltage behavior in a battery system containing hundreds of batteries [279]. A hybrid method combining an adaptive Kalman filter with DBSCAN was also reported for detecting shorted batteries in battery packs [280]. The t-distributed stochastic neighbor embedding (t-SNE) was utilized for dimensionality reduction and K-means clustering was then applied to identify thermal anomalies in battery packs [281]. Therefore, anomaly detection is well-suited for pack-level monitoring, where one abnormal battery may deviate from the statistical behavior of neighboring batteries. The same idea can also be applied to gas sensing to identify unexpected gas-release patterns, which may indicate local overheating, ISC, or accelerated side reactions.

Physics-informed hybrid learning aims to overcome the limited interpretability and poor extrapolation capability of purely data-driven models. This is particularly important when interpretability is required or when key parameters are governed by strong physical relationships, as is the case for TR, which involves coupled heat generation, electrochemical side reactions, material decomposition, gas generation, pressure buildup, venting, and thermal propagation. A data-model fusion framework has been proposed for battery fault detection by combining a single-particle electrochemical model, thermal dynamics, and Gaussian process regression, showing that machine learning can help distinguish actual faults from model uncertainty and measurement uncertainty [282]. A representative example is the chemical reaction neural network (CRNN) framework developed by Ji et al. [283] and extended by Zhang et al. [284], which uses the CRNN framework to autonomously map the unknown reaction pathways of TR gas generation. For large-scale battery systems, hybrid learning frameworks have also been developed to combine physics-guided supervised learning, unsupervised learning, and semi-supervised learning for failure prediction when labeled data are insufficient [285,286]. More broadly, physics-informed neural networks and hybrid physics-informed models have been introduced for battery modeling and prognosis [287,288]. These approaches are particularly useful for gas-evolution-based TR assessment because gas generation is strongly governed by physical and chemical mechanisms, such as electrochemical side reactions, material decomposition, heat generation, pressure buildup, and venting dynamics. This allows gas signals to be linked with heat-generation, reaction-kinetic, venting, or thermal-propagation models. Compared with black-box models, physics-informed hybrid learning can improve interpretability and may provide better generalization across battery chemistry, format, SOC, heating conditions, and abuse modes.

Beyond model architecture, an additional challenge concerns the gap between laboratory datasets and real operating data. Most published gas-evolution datasets are generated under controlled chamber, ARC, or heater-triggered conditions with relatively clean labels and stable sensing layouts. Field data, by contrast, are influenced by environmental noise, pack-level airflow and dilution, sensor drift, maintenance history, battery inconsistency, and the scarcity of true failure events. This domain gap directly affects the transferability of gas-based models from the laboratory to engineering applications. As a result, future work will likely rely more on transfer learning, domain adaptation, hybrid digital twins, and edge–cloud collaborative deployment. In such frameworks, lightweight local models can handle fast screening, while cloud-side models can perform deeper cross-scenario updating and uncertainty management [289,290].

Overall, the value of data-driven safety assessment lies not in replacing mechanistic understanding, but in integrating gas chemistry, thermal behavior, and operational context into a unified risk-evaluation framework. The most promising route is therefore a hierarchical strategy that combines chemically informed sensing at the pack edge, time-series risk screening in the BMS, and physically constrained model updating in the cloud.

5. Conclusions and outlook

5.1. Conclusions

The safety reliability of LIBs throughout their full life-cycle is essential for the widespread adoption of electric transportation and stationary energy storage. This review systematically summarizes the intrinsic correlations between gas evolution behaviors, aging mechanisms, and thermal safety boundaries in LIBs. By synthesizing experimental findings and theoretical models from recent literature, we draw the following conclusions regarding the relationship between aging and safety.

First, the composition and generation rate of gaseous byproducts serve as chemical indicators for specific aging pathways. High-temperature exposure accelerates electrolyte oxidation and cathode oxygen release, leading to a marked accumulation of carbon oxides. In contrast, low-temperature and high C-rate cycling primarily induce anode lithium plating. The highly reactive metallic lithium then reacts with binders or residual moisture, promoting hydrogen generation. Furthermore, electrical abuse conditions drive potentials beyond the stability window. This triggers severe electrolyte redox reactions and generates distinct hydrocarbon signatures. These distinct characteristics suggest that cumulative gas evolution can help infer the aging history of a LIB when interpreted together with electrochemical and thermal information.

Second, TR behaviors exhibit significant path dependence under different aging conditions. Both low-temperature and high-rate aging typically lead to lithium plating, which consistently lowers the onset temperature (T_1), accelerates the heating rate in the early stages, and shortens the intervals between T_1, T_2, and T_3. In contrast, high-temperature aging has more complex effects: depending on the temperature and duration, it can either form a temporarily protective interphase or, under more severe conditions, result in porous interphases accompanied by gas accumulation and consumption of reactive components. Although these changes collectively facilitate TR triggering, the peak heat release rate may remain unchanged due to prior active material depletion. Moreover, overcharge aging tends to destabilize the cathode and aggravate lithium plating, thereby markedly lowering T_2. However, its effects on T_3 and the peak heat-release rate remain path-dependent because reactant depletion may compete with additional electrical and thermal energy input. Over-discharge aging, on the other hand, often induces ISCs through copper dissolution, unpredictably accelerating self-heating in the early stages. This complexity highlights that safety margins are not fixed but vary according to the specific degradation path.

Third, this review highlights a framework that bridges gas-based aging diagnosis with thermal-safety prediction. By decoding gas signatures to identify the dominant aging mechanism, the current state of a LIB can be linked to its corresponding TR-risk profile. Consequently, gas analysis serves as a powerful complement to conventional aging metrics and supports proactive early-warning assessment.

Finally, data-driven methodologies provide the computational foundation for deploying this framework in practice. Machine-learning algorithms incorporating physical constraints are particularly valuable for resolving the highly nonlinear correlations between subtle gas signals and the multiphysics evolution of LIB states, thereby improving safety prognostics.

5.2. Outlook

Although significant progress has been achieved in elucidating the correlations between gas evolution and safety performance, critical challenges remain for future research, particularly concerning complex real-world operating conditions and the second-life utilization of retired LIBs. To bridge the gap between laboratory characterization and practical engineering applications, future investigations should focus on four main directions, including coupled aging mechanisms, diverse TR triggering modes, module- and pack-level translation, and advanced gas decoupling and detection technologies.

Current understanding primarily relies on single-factor aging tests, whereas actual operation involves complex coupled operating conditions. Future research should focus on gas generation mechanisms under dynamic and combined loading scenarios such as high C-rate charging under high temperature exposure or mechanical vibration coupled with electrical cycling. As highlighted by Huang et al. [290], elucidating the cross-sensitivity of gas signals under multiphysics coupling is essential for translating laboratory findings to field applications. Establishing a comprehensive database that correlates coupled aging pathways with gas evolution characteristics is a prerequisite for practical deployment.

Furthermore, the diversity of TR triggers warrants broader investigation beyond standard thermal abuse. While most existing kinetic models are derived from thermal chamber tests or ARC experiments, field failures are frequently triggered by mechanical impact or ISCs. These scenarios induce instantaneous localized heating, which drives reaction kinetics and gas evolution pathways distinct from uniform heating. Comparative studies such as the approach discussed by Finegan et al. [291] are needed to define gas signatures specific to the triggering mechanism. Future models should explicitly incorporate the influence of mechanical deformation and electrical faults on gas generation dynamics to build a more robust safety envelope.

Beyond trigger-specific gas generation, extending single-battery observations to module- and pack-level diagnostics remains a major practical challenge. Fire, smoke, and gas-release behaviors do not scale linearly with battery number, so evaluation under realistic operating and environmental conditions is needed [271]. Once gas is released from a battery, the measured signal is shaped by venting direction, enclosure geometry, airflow, dilution conditions, and the transport pathway through the surrounding module structure [292,293]. Furthermore, gas generation and the induced flow field within battery systems can substantially affect TR propagation kinetics [293,294]. During venting events, the expelled hot gas jet serves both as an observable failure signature and as an important medium for convective heat transfer [295]. When vented gases are directed toward neighboring batteries or accumulate within confined pack channels, the resulting localized heating, combustion, and explosion hazards can accelerate TR propagation across modules [271,293,294]. Conversely, directional venting and optimized exhaust pathways can mitigate gas accumulation and reduce the associated risks of propagation and explosion [292,293]. Consequently, the effectiveness of pack-level warning systems depends on multiple factors, including gas composition, sensor placement, and enclosure-scale transport dynamics between vent sources and detection points [296]. Recent system-level investigations further suggest that mechanistic principles established at the battery level require careful reinterpretation before direct application to module- and pack-level warning system design [271,292].

Finally, technical advancements in sensing and data analytics are required to decouple complex gas mixtures in real time. The capability to distinguish between aging-induced cumulative gas and abuse-induced venting gas remains a critical challenge for early warning systems. This necessitates the development of miniaturized operando sensors with high selectivity and stability. Moreover, integrating these sensors with advanced algorithms, particularly the physics-informed machine learning frameworks emphasized in this review, will be important. As suggested by Aykol et al. [297], combining high-quality sensing data with physically interpretable machine-learning models may help separate gas sources and improve the prediction of severe failure risks.

Declaration of generative AI and AI-assisted technologies in the writing process

During the preparation of this work, the authors used ChatGPT to assist with language polishing and manuscript self-checking. After using this tool, the authors reviewed and edited the content as needed, verified the scientific claims and references, and took full responsibility for the content of the publication.

Declaration of competing interest

The authors declare that they have no known competing financial interests or personal relationships that could have appeared to influence the work reported in this paper.

Acknowledgements

This research work is supported by the National Natural Science Foundation of China (Grant No. 52106261), the Shanghai Pujiang Program (24PJA058), the Open Fund of the State Key Laboratory of Environmental Adaptability for Industrial Products (Grant No. 2026EASKJ-005), and the Shanghai-Yunnan Science and Technology Collaborative Innovation Project (26HD0700400).

Data availability

Data sharing is not applicable to this article as no new data were created or analyzed in this study.

References

[1] Ahmed MD, Maraz KM. Revolutionizing energy storage: overcoming challenges and unleashing the potential of next generation lithium-ion battery technology. Mater. Eng. Res. 2023;5:265–78.
[2] Mongird K, Viswanathan V, Balducci P, Alam J, Fotedar V, Koritarov V, Hadjerioua B. An evaluation of energy storage cost and performance characteristics. Energies 2020;13:3307.
[3] Smith K, Saxon A, Keyser M, Lundstrom B, Cao Z, Roc A. Life prediction model for grid-connected Li-ion battery energy storage system. In: 2017 American control conference (ACC). IEEE; 2017. p. 4062–8.
[4] Li J, He S, Yang Q, Wei Z, Li Y, He H. A comprehensive review of second life batteries toward sustainable mechanisms: potential, challenges, and future prospects. IEEE Trans. Transp. Electrification 2022;9:4824–45.
[5] Zhao J, Feng X, Tran M-K, Fowler M, Ouyang M, Burke AF. Battery safety: fault diagnosis from laboratory to real world. J Power Sources 2024;598:234111.
[6] Mylenbusch IS, Claffey K, Chu BN. Hazards of lithium-ion battery energy storage systems (BESS), mitigation strategies, minimum requirements, and best practices. Process Saf Prog 2023;42:664–73.
[7] Zeng J, Liu S. Research on aging mechanism and state of health prediction in lithium batteries. J Energy Storage 2023;72:108274.
[8] Wang Z, Wang J. An experimental investigation of the degradation and combustion behaviors associated with lithium ion batteries after different aging treatments. J Clean Prod 2020;272:122708.
[9] Schmidt L, Hankins K, Bläubaum L, Gerasimov M, Krewer U. High temperature in situ gas analysis for identifying degradation mechanisms of lithium-ion batteries. Chem Sci 2025;16:5118–28.
[10] Wei G, Huang R, Zhang G, Jiang B, Zhu J, Guo Y, Han G, Wei X, Dai H. A comprehensive insight into the thermal runaway issues in the view of lithium-ion battery intrinsic safety performance and venting gas explosion hazards. Appl Energy 2023;349:121651.
[11] Li Z, Yao N, Yu L, Yao Y-X, Jin C-B, Yang Y, Xiao Y, Yue X-Y, Cai W-L, Xu L, et al. Inhibiting gas generation to achieve ultralong-lifespan lithium-ion batteries at low temperatures. Matter 2023;6:2274–92.
[12] Wang H, Wu S, Shao C, Luan W, Chen H. Thermal runaway and gas generation dynamics in aged lithium-ion batteries under low temperatures. J Energy Storage 2025;124:116852.

[13] Xu P, Li C, Zhu Y, Li J, Tian J, Chen Y, Wang C, Li K, Wang W, Guo S. Study on the electrochemical-thermal-gas coupling characteristics of NCM811 lithium-ion batteries under overcharging conditions. J Energy Storage 2026;141:119356.
[14] Li J, Li Y, Zeng W. Gas sensing technology as the key to safety warning of lithium-ion battery: recent advance. Sens Actuators A Phys 2024;365:114890.
[15] Qian Y, Zhao Y, Li Z, Wang Q, Zhao Y. Gas detection technology for thermal runaway of lithium-ion batteries. Front Phys 2025;13:1615872.
[16] Wang Z, Zhao Q, Sun F, Yin B, An W, Shi B. Influence of temperature dependent short-term storage on thermal runaway characteristics in lithium-ion batteries. Renew Energy 2024;232:121072.
[17] Grandjacques M, Kuntz P, Azaïs P, Genies S, Raccurt O. Thermal runaway modelling of Li-ion cells at various states of ageing with a semi-empirical model based on a kinetic equation. Batteries 2021;7:68.
[18] Wang S, Rafiz K, Liu J, Jin Y, Lin JY. Effects of lithium dendrites on thermal runaway and gassing of $LiFePO_4$ batteries. Sustain Energy Fuels 2020;4:2342–51.
[19] Börner M, Friesen A, Grützke M, Stenzel Y, Brunklaus G, Haetge J, Nowak S, Schappacher F, Winter M. Correlation of aging and thermal stability of commercial 18650-type lithium ion batteries. J Power Sources 2017;342:382–92.
[20] Wang M, Wu S, Chen Y, Luan W. The snowball effect in electrochemical degradation and safety evolution of lithium-ion batteries during long-term cycling. Appl Energy 2025;378:124909.
[21] Sun S, Brown W, Tan X, Rui B, Xiong G, Wang Y, Zeng D, Xu J. Aging matters: how degradation pathways govern thermal runaway in lithium-ion batteries. J Energy Chem 2026;114:10–21.
[22] Feng X, Ren D, He X, Ouyang M. Mitigating thermal runaway of lithium-ion batteries. Joule 2020;4:743–70.
[23] Lin Q, Fu K, Ding J, Sun K, Tan P. Advances in thermal modeling and simulation of lithium-ion batteries with machine learning approaches. Adv Intell Discov 2025;e202500147.
[24] Chen S, Zhao L, Chen K, Wu H, Yuan H, Tang W, Huang R, Wei X, Dai H. Mitigating "remaining fire"-"re-burn": multi-dimensional dynamic thermal runaway evolution mechanism and suppression for commercial lithium-ion batteries from gas perspective. Energy Storage Mater 2025;81:104520.
[25] Zhu Z, Zhang L, Wu H, Chen S, Wei X, Dai H. Wavelet packet energy proportion-based early warning for the failure of lithium-ion batteries. IEEE Trans Transp Electrif 2025;11:2219–29.
[26] Chen S, Wei X, Zhang G, Wang X, Zhu J, Feng X, Dai H, Ouyang M. All-temperature area battery application mechanism, performance, and strategies. Innovation 2023;4:100465.
[27] Han X, Lu L, Zheng Y, Feng X, Li Z, Li J, Ouyang M. A review on the key issues of the lithium ion battery degradation among the whole life cycle. eTransportation 2019;1:100005.
[28] Liu P, Yang L, Xiao B, Wang H, Li L, Ye S, Li Y, Ren X, Ouyang X, Hu J, et al. Revealing lithium battery gas generation for safer practical applications. Adv Funct Mater 2022;32:2208586.
[29] Wu K, Yang J, Liu Y, Zhang Y, Wang C, Xu J, Ning F, Wang D. Investigation on gas generation of $li_4ti_5O_{12}$/$LiNi_{1/3}co_{1/3}MN_{1/3}O_2$ cells at elevated temperature. J Power Sources 2013;237:285–90.
[30] Shi C-G, Peng X, Dai P, Xiao P, Zheng W-C, Li H-Y, Li H, Indris S, Mangold S, Hong Y-H, et al. Investigation and suppression of oxygen release by $LiNi_{0.8}co_{0.1}mn_{0.1}O_2$ cathode under overcharge conditions. Adv Energy Mater 2022;12:2200569.
[31] Zheng T, Muneeswara M, Bao H, Huang J, Zhang L, Hall DS, Boles ST, Jin W. Gas evolution in Li-ion rechargeable batteries: a review on operando sensing technologies, gassing mechanisms, and emerging trends. Chemelectrochem 2024;11:e202400065.
[32] Metzger M, Strehle B, Solchenbach S, Gasteiger HA. Origin of H_2 evolution in LIBs: H_2O reduction vs. electrolyte oxidation. J Electrochem Soc 2016;163:A798.
[33] Misiewicz C, Lundström R, Ahmed I, Lacey MJ, Brant WR, Berg EJ. Online electrochemical mass spectrometry on large-format Li-ion cells. J Power Sources 2023;554:232318.
[34] Ellis L, Allen J, Thompson L, Harlow J, Stone W, Hill I, Dahn J. Quantifying, understanding and evaluating the effects of gas consumption in lithium-ion cells. J Electrochem Soc 2017;164:A3518.
[35] Stenzel YP, Horsthemke F, Winter M, Nowak S. Chromatographic techniques in the research area of lithium ion batteries: current state-of-the-art. Separations 2019;6:26.
[36] Forestier C, Lecocq A, Zantman A, Grugeon S, Sannier L, Marlair G, Laruelle S. Study of the role of $LiNi_{1/3}MN_{1/3}co_{1/3}O_2$/graphite Li-ion pouch cells confinement, electrolyte composition and separator coating on thermal runaway and off-gas toxicity. J Electrochem Soc 2020;167:090513.
[37] Gerelt-Od B, Kim H, Lee UJ, Kim J, Kim N, Han YJ, Son H, Yoon S. Potential dependence of gas evolution in 18650 cylindrical lithium-ion batteries using in-situ Raman spectroscopy. J Electrochem Soc 2018;165:A168.
[38] Deng J, Yu X, Pang D, Fei B, Mo J. Cutting-edge gas sensor design for monitoring thermal runaway in lithium-ion batteries: a critical review. J Energy Chem 2025;109:769–85.
[39] Zhang G, Wei X, Chen S, Wei G, Zhu J, Wang X, Han G, Dai H. Research on the impact of high-temperature aging on the thermal safety of lithium-ion batteries. J Energy Chem 2023;87:378–89.
[40] Gerelt-Od B, Kim J, Shin E, Kang H, Kim N, Jo C, Son H, Yoon S. In situ Raman investigation of resting thermal effects on gas emission in charged commercial 18650 lithium ion batteries. J Ind Eng Chem 2021;96:339–44.
[41] Cai Q, Ji Q, Chen X, Wang T, Li L, Yuan Q, Gao S, Cheng Y-J. Comprehensive study of high-temperature calendar aging on cylinder Li-ion battery. Chem Eng Sci 2024;298:120355.
[42] Cao Y, Li N, Yuan K, Li N, Zhang W, Liang S, Hou Z, Lei D, Jin T, Wang J-G, et al. Revealing the mechanisms of electrolyte additive PTS on ni-rich electrode: tolerance to high temperature (50 °C) and high voltage (4.6 V). Energy Storage Mater 2023;60:102851.
[43] Lee KH, Song EH, Lee JY, Jung BH, Lim HS. Mechanism of gas build-up in a Li-ion cell at elevated temperature. J Power Sources 2004;132:201–5.
[44] Hall DS, Eldesoky A, Logan E, Tonita EM, Ma X, Dahn J. Exploring classes of co-solvents for fast-charging lithium-ion cells. J Electrochem Soc 2018;165:A2365.
[45] Strehle B, Friedrich F, Gasteiger HA. A comparative study of structural changes during long-term cycling of NCM-811 at ambient and elevated temperatures. J Electrochem Soc 2021;168:050512.
[46] Spotte-Smith EWC, Vijay S, Petrocelli TB, Rinkel BL, McCloskey BD, Persson KA. A critical analysis of chemical and electrochemical oxidation mechanisms in Li-ion batteries. J Phys Chem Lett 2024;15:391–400.
[47] Chang M, Cheng F, Zhang W, Liao M, Li Q, Fang C, Han J. Integrated oxygen-constraining strategy for ni-rich layered oxide cathodes. ACS Nano 2024;19:712–21.
[48] Ng B, Coman PT, Faegh E, Peng X, Karakalos SG, Jin X, Mustain WE, White RE. Low-temperature lithium plating/corrosion hazard in lithium-ion batteries: electrode rippling, variable states of charge, and thermal and nonthermal runaway. ACS Appl Energy Mater 2020;3:3653–64.
[49] Vilá RA, Boyle DT, Dai A, Zhang W, Sayavong P, Ye Y, Yang Y, Dionne JA, Cui Y. LiH formation and its impact on li batteries revealed by cryogenic electron microscopy. Sci Adv 2023;9:eadf3609.
[50] Taskovic T, Thompson L, Eldesoky A, Lumsden M, Dahn J. Optimizing electrolyte additive loadings in NMC532/graphite cells: vinylene carbonate and ethylene sulfate. J Electrochem Soc 2021;168:010514.
[51] Guillot SL, Usrey ML, Peña-Hueso A, Kerber BM, Zhou L, Du P, Johnson T. Reduced gassing in lithium-ion batteries with organosilicon additives. J Electrochem Soc 2021;168:030533.
[52] Zhang G, Shen W, Wei X. Lithium-ion battery thermal safety evolution during high-temperature nonlinear aging. Fuel 2024;362:130845.
[53] Xiong D, Petibon R, Nie M, Ma L, Xia J, Dahn JR. Interactions between positive and negative electrodes in Li-ion cells operated at high temperature and high voltage. J Electrochem Soc 2016;163:A546.
[54] Lüchtefeld J, Lee M-Y, Hemmelmann H, Wachs S, Behling C, Mayrhofer KJ, Elm MT, Berkes BB. Contribution of electrolyte decomposition products and the effect of temperature on the dissolution of transition metals from cathode materials. ACS Omega 2023;8:32606–14.
[55] Kim Y. Mechanism of gas evolution from the cathode of lithium-ion batteries at the initial stage of high-temperature storage. J Mater Sci 2013;48:8547–51.
[56] Hu D, Chen L, Tian J, Su Y, Li N, Chen G, Hu Y, Dou Y, Chen S, Wu F. Research progress of lithium plating on graphite anode in lithium-ion batteries. Chin. J. Chem. 2021;39:165–73.
[57] Janakiraman U, Garrick TR, Fortier ME. Lithium plating detection methods in Li-ion batteries. J Electrochem Soc 2020;167:160552.
[58] Brown DE, McShane EJ, Konz ZM, Knudsen KB, McCloskey BD. Detecting onset of lithium plating during fast charging of Li-ion batteries using operando electrochemical impedance spectroscopy. Cell Rep Phys Sci 2021;2.
[59] Song M, Lee D, Kim J, Heo Y, Nam C, Ko D, Lim J. Chemical decomposition pathway of residual lithium carbonate of Li-ion battery cathodes. J Power Sources 2023;560:232699.
[60] Mei W, Jiang L, Liang C, Sun J, Wang Q. Understanding of li-plating on graphite electrode: detection, quantification and mechanism revelation. Energy Storage Mater 2021;41:209–21.
[61] Wang X, Zhang M, Alvarado J, Wang S, Sina M, Lu B, Bouwer J, Xu W, Xiao J, Zhang J-G, et al. New insights on the structure of electrochemically deposited lithium metal and its solid electrolyte interphases via cryogenic TEM. Nano Lett 2017;17:7606–12.
[62] Xiang Y, Tao M, Chen X, Shan P, Zhao D, Wu J, Lin M, Liu X, He H, Zhao W, et al. Gas induced formation of inactive li in rechargeable lithium metal batteries. Nat Commun 2023;14:177.
[63] Xu G, Li J, Wang C, Du X, Lu D, Xie B, Wang X, Lu C, Liu H, Dong S, et al. Ed. The formation/decomposition equilibrium of LiH and its contribution on anode failure in practical lithium metal batteries. Angew. Chem. Int. 2021;133:7849–55.
[64] Wang S, Hu C, Yu R, Sun Z, Jin Y. Study on low-temperature cycle failure mechanism of a ternary lithium ion battery. RSC Adv 2022;12:20755–61.
[65] Edge JS, O'Kane S, Prosser R, Kirkaldy ND, Patel AN, Hales A, Ghosh A, Ai W, Chen J, Yang J, et al. Lithium ion battery degradation: what you need to know. Phys Chem Chem Phys 2021;23:8200–21.
[66] Miao J. Review on electrode degradation at fast charging of Li-ion and li metal batteries from a kinetic perspective. Electrochem 2023;4:156–80.
[67] Mattinen U, Klett M, Lindbergh G, Lindström RW. Gas evolution in commercial Li-ion battery cells measured by on-line mass spectrometry–effects of C-rate and cell voltage. J Power Sources 2020;477:228968.
[68] Yang Z, Li X, Li J, Li H, Shi J, Fan X, Cong Z, Feng X, Yang X-G. Study on influencing factors of calendar aging and cycle aging of LFP batteries. Appl Sci 2025;15:12749.
[69] Kaufman LA, Huang T-Y, Lee D, McCloskey BD. Particle surface cracking is correlated with gas evolution in high-ni Li-ion cathode materials. ACS Appl Mater Interfaces 2022;14:39959–64.
[70] Parikh D, Geng L, Lyu H, Jafta CJ, Liu H, Meyer III HM, Chen J, Sun X-G, Dai S, Li J. Operando analysis of gas evolution in $TiNb_2O_7$ (TNO)-based anodes for advanced high-energy lithium-ion batteries under fast charging. ACS Appl Mater Interfaces 2021;13:55145–55.
[71] Peng Y, Ding M, Zhang K, Zhang H, Hu Y, Lin Y, Hu W, Liao Y, Tang S, Liang J, et al. Quantitative analysis of the coupled mechanisms of lithium plating, SEI

growth, and electrolyte decomposition in fast charging battery. ACS Energy Lett 2024;9:6022–8.
[72] Liu Q, Xiong D, Petibon R, Du C, Dahn J. Gas evolution during unwanted lithium plating in Li-ion cells with EC-based or EC-free electrolytes. J Electrochem Soc 2016;163:A3010.
[73] Ohsaki T, Kishi T, Kuboki T, Takami N, Shimura N, Sato Y, Sekino M, Satoh A. Overcharge reaction of lithium-ion batteries. J Power Sources 2005;146:97–100.
[74] Mao Z, Farkhondeh M, Pritzker M, Fowler M, Chen Z. Calendar aging and gas generation in commercial graphite/NMC-LMO lithium-ion pouch cell. J Electrochem Soc 2017;164:A3469.
[75] Xie Y, Li C, Wu T, Tang R, Hu Y, Zhu Y, Qiu H, Zhang R. Analysis of energy storage battery degradation under different electrical stress levels. Case Stud Therm Eng 2025;106355.
[76] Du H, Wang Y, Kang Y, Zhao Y, Tian Y, Wang X, Tan Y, Liang Z, Wozny J, Li T, et al. Side reactions/changes in lithium-ion batteries: mechanisms and strategies for creating safer and better batteries. Adv Mater 2024;36:2401482.
[77] Ouyang D, Chen M, Liu J, Wei R, Weng J, Wang J. Investigation of a commercial lithium-ion battery under overcharge/over-discharge failure conditions. RSC Adv 2018;8:33414–24.
[78] Mao N, Geng X, Liu Y, Huang X, Hao M. Degradation behavior and underlying mechanisms of electrochemical and thermal stability in li $(ni_{0.5}mn_{0.3}co_{0.2})O_2$/graphite lithium-ion batteries under overcharge conditions. Int Commun Heat Mass Transf 2026;170:110029.
[79] Jung R, Metzger M, Maglia F, Stinner C, Gasteiger HA. Oxygen release and its effect on the cycling stability of $LiNi_xmn_yco_zO_2$ (NMC) cathode materials for Li-ion batteries. J Electrochem Soc 2017;164:A1361.
[80] Kong W, Li H, Huang X, Chen L. Gas evolution behaviors for several cathode materials in lithium-ion batteries. J Power Sources 2005;142:285–91.
[81] Mao C, Ruther RE, Geng L, Li Z, Leonard DN, Meyer III HM, Sacci RL, Wood III DL. Evaluation of gas formation and consumption driven by crossover effect in high-voltage lithium-ion batteries with ni-rich NMC cathodes. ACS Appl Mater Interfaces 2019;11:43235–43.
[82] Guo Q, Liu S, Zhang J, Huang Z, Han D. Effects of charging rates on heat and gas generation in lithium-ion battery thermal runaway triggered by high temperature coupled with overcharge. J Power Sources 2024;600:234237.
[83] Wen J, Yu Y, Chen C. A review on lithium-ion batteries safety issues: existing problems and possible solutions. Mater. Express 2012;2:197–212.
[84] Liu Y, Han W, Wang L, Chang Y, Huo S, Liu S, He X. Mechanisms and safety risks of lithium-ion battery over-discharge: consequences and prevention control. Nano Res 2026;19:94908060.
[85] Vetter J, Novák P, Wagner MR, Veit C, Möller K-C, Besenhard J, Winter M, Wohlfahrt-Mehrens M, Vogler C, Hammouche A. Ageing mechanisms in lithium-ion batteries. J Power Sources 2005;147:269–81.
[86] Long Z, Chen K, Tang M, Zheng X, Wang H, Luo Y, Li Y, Nie G, Zhang X, Gao G, et al. A review of modeling the aging mechanism of LIBs: multi-physics field coupling analysis from LLI to LAM. Int J Green Energy 2026;1–28.
[87] Song Y, Wang L, Sheng L, Ren D, Liang H, Li Y, Wang A, Zhang H, Xu H, He X. The significance of mitigating crosstalk in lithium-ion batteries: a review. Energy Environ Sci 2023;16:1943–63.
[88] Sharifi-Asl S, Lu J, Amine K, Shahbazian-Yassar R. Oxygen release degradation in Li-ion battery cathode materials: mechanisms and mitigating approaches. Adv Energy Mater 2019;9:1900551.
[89] Ping P, Wang Q, Huang P, Li K, Sun J, Kong D, Chen C. Study of the fire behavior of high-energy lithium-ion batteries with full-scale burning test. J Power Sources 2015;285:80–9.
[90] Dahn J, Fuller E, Obrovac M, Von Sacken U. Thermal stability of li_xCoO_2, li_xNiO_2 and λ-MnO_2 and consequences for the safety of Li-ion cells. Solid State Ion 1994;69:265–70.
[91] Salomez B, Grugeon S, Armand M, Tran-Van P, Laruelle S. Gassing mechanisms in lithium-ion battery. J Electrochem Soc 2023;170:050537.
[92] Ma X, Yu J, Dong Q, Zou X, Zheng L, Hu Y, Shen Y, Chen L, Yan F. Ionic liquid-type additive for lithium metal batteries operated in $LiPF_6$ based-electrolyte containing 2500 ppm H_2O. ACS Appl Mater Interfaces 2022;14:41103–13.
[93] Freiberg AT, Sicklinger J, Solchenbach S, Gasteiger HA. Li_2CO_3 decomposition in Li-ion batteries induced by the electrochemical oxidation of the electrolyte and of electrolyte impurities. Electrochim Acta 2020;346:136271.
[94] Martinez AC, Grugeon S, Cailleu D, Courty M, Tran-Van P, Delobel B, Laruelle S. High reactivity of the nickel-rich $LiNi_{1-x-y}mn_xco_yO_2$ layered materials surface towards H_2O/CO_2 atmosphere and $LiPF_6$-based electrolyte. J Power Sources 2020;468:228204.
[95] Vajo JJ, Skeith SL, Mertens F, Jorgensen SW. Hydrogen-generating solid-state hydride/hydroxide reactions. J Alloys Compd 2005;390:55–61.
[96] Hatsukade T, Schiele A, Hartmann P, Brezesinski T, Janek J. Origin of carbon dioxide evolved during cycling of nickel-rich layered NCM cathodes. ACS Appl Mater Interfaces 2018;10:38892–9.
[97] Cao D, Tan C, Chen Y. Oxidative decomposition mechanisms of lithium carbonate on carbon substrates in lithium battery chemistries. Nat Commun 2022;13:4908.
[98] Petibon R, Rotermund L, Dahn J. Evaluation of phenyl carbonates as electrolyte additives in lithium-ion batteries. J Power Sources 2015;287:184–95.
[99] Bernhard R, Metzger M, Gasteiger HA. Gas evolution at graphite anodes depending on electrolyte water content and SEI quality studied by on-line electrochemical mass spectrometry. J Electrochem Soc 2015;162:A1984.
[100] Metzger M, Marino C, Sicklinger J, Haering D, Gasteiger HA. Anodic oxidation of conductive carbon and ethylene carbonate in high-voltage Li-ion batteries quantified by on-line electrochemical mass spectrometry. J Electrochem Soc 2015;162:A1123.
[101] Solchenbach S, Metzger M, Egawa M, Beyer H, Gasteiger HA. Quantification of PF_5 and POF_3 from side reactions of $LiPF_6$ in Li-ion batteries. J Electrochem Soc 2018;165:A3022.
[102] Strmcnik D, Castelli IE, Connell JG, Haering D, Zorko M, Martins P, Lopes PP, Genorio B, Østergaard T, Gasteiger HA, et al. Electrocatalytic transformation of HF impurity to H_2 and LiF in lithium-ion batteries. Nat Catal 2018;1:255–62.
[103] Shiraishi S, Kanamura K, Takehara Z-I. Study of the surface composition of highly smooth lithium deposited in various carbonate electrolytes containing HF. Langmuir 1997;13:3542–9.
[104] Agubra VA, Fergus JW. The formation and stability of the solid electrolyte interface on the graphite anode. J Power Sources 2014;268:153–62.
[105] Han J-G, Kim K, Lee Y, Choi N-S. Scavenging materials to stabilize $LiPF_6$-containing carbonate-based electrolytes for Li-ion batteries. Adv Mater 2019;31:1804822.
[106] Martins M, Haering D, Connell JG, Wan H, Svane KL, Genorio B, Farinazzo Bergamo Dias Martins P, Lopes PP, Gould B, Maglia F, et al. Role of catalytic conversions of ethylene carbonate, water, and HF in forming the solid-electrolyte interphase of Li-ion batteries. ACS Catal 2023;13:9289–301.
[107] Kim S, Kim H-S, Kim B, Kim Y-J, Jung J-W, Ryu W-H. In situ gas analysis by differential electrochemical mass spectrometry for advanced rechargeable batteries: a review. Adv Energy Mater 2023;13:2301983.
[108] Roen L, Paik C, Jarvi T. Electrocatalytic corrosion of carbon support in PEMFC cathodes. Electrochem Solid-State Lett 2003;7:A19.
[109] Solchenbach S, Hong G, Freiberg ATS, Jung R, Gasteiger HA. Electrolyte and SEI decomposition reactions of transition metal ions investigated by on-line electrochemical mass spectrometry. J Electrochem Soc 2018;165:3304–12.
[110] Rinkel BL, Vivek JP, Garcia-Araez N, Grey CP. Two electrolyte decomposition pathways at nickel-rich cathode surfaces in lithium-ion batteries. Energy Environ Sci 2022;15:3416–38.
[111] Rinkel BL, Hall DS, Temprano I, Grey CP. Electrolyte oxidation pathways in lithium-ion batteries. J Am Chem Soc 2020;142:15058–74.
[112] Dose WM, Li W, Temprano I, O'Keefe CA, Mehdi BL, De Volder MF, Grey CP. Onset potential for electrolyte oxidation and ni-rich cathode degradation in lithium-ion batteries. ACS Energy Lett 2022;7:3524–30.
[113] Jung R, Metzger M, Maglia F, Stinner C, Gasteiger HA. Chemical versus electrochemical electrolyte oxidation on NMC111, NMC622, NMC811, LNMO, and conductive carbon. J Phys Chem Lett 2017;8:4820–5.
[114] Wandt J, Freiberg AT, Ogrodnik A, Gasteiger HA. Singlet oxygen evolution from layered transition metal oxide cathode materials and its implications for lithium-ion batteries. Mater Today 2018;21:825–33.
[115] Heiskanen SK, Kim J, Lucht BL. Generation and evolution of the solid electrolyte interphase of lithium-ion batteries. Joule 2019;3:2322–33.
[116] An SJ, Li J, Daniel C, Mohanty D, Nagpure S, Wood III DL. The state of understanding of the lithium-ion-battery graphite solid electrolyte interphase (SEI) and its relationship to formation cycling. Carbon 2016;105:52–76.
[117] Nie M, Lucht BL. Role of lithium Salt on solid electrolyte interface (SEI) formation and structure in lithium ion batteries. J Electrochem Soc 2014;161:1001–6.
[118] Wang Y, Nakamura S, Ue M, Balbuena PB. Theoretical studies to understand surface chemistry on carbon anodes for lithium-ion batteries: reduction mechanisms of ethylene carbonate. J Am Chem Soc 2001;123:11708–18.
[119] Nie Q, Liu Z, Cheng M, Pei S, Yang D, Cheng C, Guo D, Yang M. Platinum coated capillary enhanced gas Raman spectroscopy: analyzing the multi-gas release from lithium-ion batteries after formation. IEEE Sens J 2025;25:18032–40.
[120] Li JL, Wang YN, Sun SY, Zheng Z, Gao Y, Shi P, Zhao YJ, Li X, Li Q, Zhang XQ, Huang JQ. Understanding and regulating the mechanical stability of solid electrolyte interphase in batteries. Adv Energy Mater 2025;15:2403845.
[121] Metzger M, Strehle B, Solchenbach S, Gasteiger HA. Hydrolysis of ethylene carbonate with water and hydroxide under battery operating conditions. J Electrochem Soc 2016;163:1219–25.
[122] Harris OC, Lee SE, Lees C, Tang M. mechanisms and consequences of chemical cross-talk in advanced Li-ion batteries. J Phys Energy 2020;2:032002.
[123] Gilbert JA, Shkrob IA, Abraham DP. Transition metal dissolution, ion migration, electrocatalytic reduction and capacity loss in lithium-ion full cells. J Electrochem Soc 2017;164:A389.
[124] Li W. An unpredictable hazard in lithium-ion batteries from transition metal ions: dissolution from cathodes, deposition on anodes and elimination strategies. J Electrochem Soc 2020;167:090514.
[125] Zhan C, Wu T, Lu J, Amine K. Dissolution, migration, and deposition of transition metal ions in Li-ion batteries exemplified by MN-based cathodes–a critical review. Energy Environ Sci 2018;11:243–57.
[126] Sloop SE, Kerr JB, Kinoshita K. The role of Li-ion battery electrolyte reactivity in performance decline and self-discharge. J Power Sources 2003;119:330–7.
[127] Prempluem S, Sangsanit T, Santiyuk K, Homlamai K, Tejangkura W, Songthan R, Anansuksawat N, Sawangphruk M. Complex reaction mechanisms of electrolyte decomposition at large-scale ni-rich Li-ion battery cells including electrode crosstalk effect. J Power Sources 2024;606:234538.
[128] Lin F, Markus IM, Nordlund D, Weng T-C, Asta MD, Xin HL, Doeff MM. Surface reconstruction and chemical evolution of stoichiometric layered cathode materials for lithium-ion batteries. Nat Commun 2014;5:3529.
[129] Xu C, Märker K, Lee J, Mahadevegowda A, Reeves PJ, Day SJ, Groh MF, Emge SP, Ducati C, Layla Mehdi B, et al. Bulk fatigue induced by surface reconstruction in layered ni-rich cathodes for Li-ion batteries. Nat Mater 2021;20:84–92.
[130] Shen J, Zhou M, Tang W, Huang Q, Pi H, Liu W, Liu R, Li L. Surface reconstruction strategy enables rapid upcycling highly degraded layered cathode. Nano Energy 2025;136:110741.
[131] Huang Y, Su D, Zheng L, Yang G, Li K, Jiang J, Pan Q, Hu S, Li Y, Li Q, et al. Lattice-compatible piezoelectric modification for suppressing lattice oxygen

evolution of ni-rich cathode materials at high cut-off voltage. Energy Storage Mater 2024;71:103678.
[132] Suk S, Yoo N, Lee Y, Kwon J, Ahn H, Yoo S, Lee J, Kim H, Bae J, Kim J, et al. Understanding cross-talk–induced anode slippage in high-voltage mid-ni NCM/graphite full cells. Sci Technol Adv Mater 2025;26:2502324.
[133] Wang Z, Zhao Q, Wang S, Song Y, Shi B, He J. Aging and post-aging thermal safety of lithium-ion batteries under complex operating conditions: a comprehensive review. J Power Sources 2024;623:235453.
[134] Ren D, Hsu H, Li R, Feng X, Guo D, Han X, Lu L, He X, Gao S, Hou J, et al. A comparative investigation of aging effects on thermal runaway behavior of lithium-ion batteries. eTransportation 2019;2:100034.
[135] Liu X, Yin L, Ren D, Wang L, Ren Y, Xu W, Lapidus S, Wang H, He X, Chen Z, et al. In situ observation of thermal-driven degradation and safety concerns of lithiated graphite anode. Nat Commun 2021;12:4235.
[136] Yu S, Mao Y, Xie J, Xu C, Lu T. Thermal runaway chain reaction determination and mechanism model establishment of NCA-graphite battery based on the internal temperature. Appl Energy 2024;353:122097.
[137] Jia Z, Qin P, Li Z, Wei Z, Jin K, Jiang L, Wang Q. Analysis of gas release during the process of thermal runaway of lithium-ion batteries with three different cathode materials. J Energy Storage 2022;50:104302.
[138] Liu Y, Ju L, zhuang Jia Z, Cheng Z, Min Y, Mei W, Qin P, Wang Q. Experimental study on the internal pressure evolution of large-format $LiFePO_4$ battery during thermal runaway. J Energy Storage 2024;102:114196.
[139] Aurbach D, Zaban A, Ein-Eli Y, Weissman I, Chusid O, Markovsky B, Levi M, Levi E, Schechter A, Granot E. Recent studies on the correlation between surface chemistry, morphology, three-dimensional structures and performance of li and li-C intercalation anodes in several important electrolyte systems. J Power Sources 1997;68:91–8.
[140] Peng R, Kong D, Ping P, Wang G, Gao X, Lv H, Zhao H, He X, Zhang Y, Dai X. Thermal runaway modeling of lithium-ion batteries at different scales: recent advances and perspectives. Energy Storage Mater 2024;103417.
[141] Senthil C, Subramani A, Gupta RK, Sofer Z. Functional electrolyte additives: a pinch of Salt/solvent to an electrolyte for high energy density lithium-ion and lithium–metal batteries. Small 2025;21:2504276.
[142] Feng X, Ouyang M, Liu X, Lu L, Xia Y, He X. Thermal runaway mechanism of lithium ion battery for electric vehicles: a review. Energy Storage Mater 2018;10:246–67.
[143] Du Pasquier A, Disma F, Bowmer T, Gozdz A, Amatucci G, Tarascon J-M. Differential scanning calorimetry study of the reactivity of carbon anodes in plastic Li-ion batteries. J Electrochem Soc 1998;145:472.
[144] Huang Z, Zhao C, Li H, Peng W, Zhang Z, Wang Q. Experimental study on thermal runaway and its propagation in the large format lithium ion battery module with two electrical connection modes. Energy 2020;205:117906.
[145] Spotnitz R, Franklin J. Abuse behavior of high-power, lithium-ion cells. J Power Sources 2003;113:81–100.
[146] Nakhanivej P, Rana HH, Kim H, Xia BY, Park HS. Transport and durability of energy storage materials operating at high temperatures. ACS Nano 2020;14:7696–703.
[147] Yuan Q, Zhao F, Wang W, Zhao Y, Liang Z, Yan D. Overcharge failure investigation of lithium-ion batteries. Electrochim Acta 2015;178:682–8.
[148] Geisbauer C, Wöhrl K, Mittmann C, Schweiger H-G. Review of safety aspects of calendar aged lithium ion batteries. J Electrochem Soc 2020;167:090523.
[149] Shi D, Cui Y, Shen X, Gao Z, Ma X, Li X, Fang Y, Wang S, Fang S. A review of the combined effects of environmental and operational factors on lithium-ion battery performance: temperature, vibration, and charging/discharging cycles. RSC Adv 2025;15:13272–83.
[150] Hawkins BE, Asare H, Chen B, Messinger RJ, West W, Jones J-P. Elucidating failure mechanisms in Li-ion batteries operating at 100°C. J Electrochem Soc 2023;170:100522.
[151] Xie W, Liu X, He R, Li Y, Gao X, Li X, Peng Z, Feng S, Feng X, Yang S. Challenges and opportunities toward fast-charging of lithium-ion batteries. J Energy Storage 2020;32:101837.
[152] Essl C, Golubkov AW, Fuchs A. Influence of aging on the failing behavior of automotive lithium-ion batteries. Batteries 2021;7:23.
[153] Feng Y, Zhou L, Ma H, Wu Z, Zhao Q, Li H, Zhang K, Chen J. Challenges and advances in wide-temperature rechargeable lithium batteries. Energy Environ Sci 2022;15:1711–59.
[154] Gao T, Bai J, Ouyang D, Wang Z, Bai W, Mao N, Zhu Y. Effect of aging temperature on thermal stability of lithium-ion batteries: Part A–High-temperature aging. Renew Energy 2023;203:592–600.
[155] Waldmann T, Quinn JB, Richter K, Kasper M, Tost A, Klein A, Wohlfahrt-Mehrens M. Electrochemical, post-mortem, and ARC analysis of Li-ion cell safety in second-life applications. J Electrochem Soc 2017;164:A3154.
[156] Roth E, Doughty D. Thermal abuse performance of high-power 18650 Li-ion cells. J Power Sources 2004;128:308–18.
[157] García A, Monsalve-Serrano J, de Vargas Lewiski F, Golke D. Characterization of pristine and aged NMC lithium-ion battery thermal runaway using ARC experiments coupled with optical techniques. Appl Therm Eng 2024;257:124244.
[158] Zhang J, Su L, Li Z, Sun Y, Wu N. The evolution of lithium-ion cell thermal safety with aging examined in a battery testing calorimeter. Batteries 2016;2:12.
[159] Liu J, Zhou L, Zhang Y, He T, Wang Z. Thermal stability of lithium-ion battery subjected to inhomogeneous aging. Process Saf Environ Prot 2023;180:992–1002.
[160] Wang Q, Sun J, Yao X, Chen C. Thermal behavior of lithiated graphite with electrolyte in lithium-ion batteries. J Electrochem Soc 2005;153:A329.
[161] Feng X, He X, Ouyang M, Wang L, Lu L, Ren D, Santhanagopalan S. A coupled electrochemical-thermal failure model for predicting the thermal runaway behavior of lithium-ion batteries. J Electrochem Soc 2018;165:3748–65.
[162] Zhang G, Chen S, Zhu J, Dai H, Wei X. Investigation on the impact of high-temperature calendar and cyclic aging on battery overcharge performance. SAE Int J Adv Curr Pract Mobil 2022;4:1953–60.
[163] Kadir M, Rani M, Razlan Z, Shahriman A, Kamarrudin N, Yinn W, Akmal A, Uda MA, Gautier Y. Beyond limits: short review on temperature's role in characterizing lithium-ion battery performance. In: J. Phys. Conf. Ser. 2928. IOP Publishing; 2024, p. 012014.
[164] Zhang G, Wei X, Chen S, Zhu J, Dai H. Comprehensively investigating the impact of high-temperature cyclic aging on thermal runaway characteristics for lithium-ion batteries. Technical Report SAE Technical Paper; 2022.
[165] Feng X, Ren D, Zhang S, He X, Wang L, Ouyang M. Influence of aging paths on the thermal runaway features of lithium-ion batteries in accelerating rate calorimetry tests. Int J Electrochem Sci 2019;14:44–58.
[166] Chu Y, Wang B. Investigation of thermal runaway mechanism of secondary $li(ni_{0.5}co_{0.3}mn_{0.2})o_2$ batteries. In: J. Phys. Conf. Ser. 2954. IOP Publishing; 2025, p. 012130.
[167] Taniguchi S, Shironita S, Konakawa K, Mendoza-Hernandez OS, Sone Y, Umeda M. Thermal characteristics of 80 C storage-degraded 18650-type lithium-ion secondary cells. J Power Sources 2019;416:148–54.
[168] Wang S, Wang Q, Xu L, Sun Y, Feng X, Wang H. A review on mechanisms, characteristics and relating hazards of vent gases from thermally abused Li-ion batteries. J Energy Storage 2024;84:110892.
[169] Lammer M, Königseder A, Gluschitz P, Hacker V. Influence of aging on the heat and gas emissions from commercial lithium ion cells in case of thermal failure. J. Electrochem. Sci. Eng. 2018;8:101–10.
[170] Guo J, Ping P, Ren J, Ren X, Gao W, Kong D, Wang D, Feng Z. High-temperature calendar aging at low state-of-charge: electrochemical degradation, thermal safety implications, and optimal SOC ranges for lithium-ion battery storage and transport. J Energy Storage 2025;125:116988.
[171] Zhang G, Wei X, Han G, Dai H, Zhu J, Wang X, Tang X, Ye J. Lithium plating on the anode for lithium-ion batteries during long-term low temperature cycling. J Power Sources 2021;484:229312.
[172] Lin X, Khosravinia K, Hu X, Li J, Lu W. Lithium plating mechanism, detection, and mitigation in lithium-ion batteries. Prog Energy Combust Sci 2021;87:100953.
[173] Waldmann T, Hogg B-I, Wohlfahrt-Mehrens M. Li plating as unwanted side reaction in commercial Li-ion cells–a review. J Power Sources 2018;384:107–24.
[174] Ouyang D, Weng J, Chen M, Wang J, Wang Z. Electrochemical and thermal characteristics of aging lithium-ion cells after long-term cycling at abusive-temperature environments. Process Saf Environ Prot 2022;159:1215–23.
[175] Friesen A, Horsthemke F, Mönnighoff X, Brunklaus G, Krafft R, Börner M, Risthaus T, Winter M, Schappacher FM. Impact of cycling at low temperatures on the safety behavior of 18650-type lithium ion cells: combined study of mechanical and thermal abuse testing accompanied by post-mortem analysis. J Power Sources 2016;334:1–11.
[176] Friesen A, Hildebrand S, Horsthemke F, Börner M, Klöpsch R, Niehoff P, Schappacher FM, Winter M. Al_2O_3 coating on anode surface in lithium ion batteries: impact on low temperature cycling and safety behavior. J Power Sources 2017;363:70–7.
[177] Wu S, Wang C, Luan W, Zhang Y, Chen Y, Chen H. Thermal runaway behaviors of Li-ion batteries after low temperature aging: experimental study and predictive modeling. J Energy Storage 2023;66:107451.
[178] Cai Z, Mendoza S, Goodman J, McGann J, Han B, Sanchez H, Spray R. The influence of cycling, temperature, and electrode gapping on the safety of prismatic lithium-ion batteries. J Electrochem Soc 2020;167:160515.
[179] Qi C, Liu Z, Lin C, Hu Y, Liu D, Li Z, Yi A. Study on the effect of low-temperature cycling on the thermal and gas production behaviors of $ni_{0.8}co_{0.1}al_{0.1}$/graphite lithium-ion batteries. Appl Therm Eng 2024;247:123054.
[180] Abd-El-Latif AA, Sichler P, Kasper M, Waldmann T, Wohlfahrt-Mehrens M. Insights into thermal runaway of Li-ion cells by accelerating rate calorimetry coupled with external sensors and online gas analysis. Batter Supercaps 2021;4:1135–44.
[181] Ma Y, Chiang SW, Chu X, Li J, Gan L, Xu C, Yao Y, He Y, Li B, Kang F, et al. Thermal design and optimization of lithium ion batteries for unmanned aerial vehicles. Energy Storage 2019;1:e48.
[182] Wang Y, Sun Y, Zhang Y, Chen X, Shen H, Liu Y, Zhang X, Zhang Y. Optimal modeling and analysis of microgrid lithium iron phosphate battery energy storage system under different power supply states. J Power Sources 2022;521:230931.
[183] Huang Y, Zhao Y, Xu W, Bai W, Shen X, Wang J, Lu Y, Wang Z. Study on the influence of high-rate charge/discharge cycle numbers and spacing on thermal runaway propagation in lithium-ion batteries. J Energy Storage 2025;115:116005.
[184] Ouyang D, Weng J, Chen M, Wang J, Wang Z. Electrochemical and thermal features of aging lithium-ion batteries cycled at various current rates. J Loss Prev Process Ind 2023;85:105156.
[185] Zhang G, Wei X, Chen S, Zhu J, Han G, Wang X, Dai H. Revealing the impact of fast charge cycling on the thermal safety of lithium-ion batteries. ACS Appl Energy Mater 2022;5:7056–68.
[186] Wang Z, Wu X, Bai Z, Yang N, Guo G, Banjoko OS. Enhancing fast charging performance of lithium-ion batteries: the role of operating temperature and charging rate. Electrochim Acta 2025;511:145390.
[187] Sun S, Guan T, Cheng X, Zuo P, Gao Y, Du C, Yin G. Accelerated aging and degradation mechanism of $LiFePO_4$/graphite batteries cycled at high discharge rates. RSC Adv 2018;8:25695–703.
[188] Bichon A, Geniès S, Azaïs P, Buzon D, Raccurt O. Operando detection of lithium plating and stripping in fast-charging Li-ion cells with a reference electrode. Batter Supercaps 2025;2500071.

[189] Qu J, Jiang Z, Zhang J. Investigation on lithium-ion battery degradation induced by combined effect of current rate and operating temperature during fast charging. J Energy Storage 2022;52:104811.

[190] Ouyang D, Weng J, Chen M, Wang J. Impact of high-temperature environment on the optimal cycle rate of lithium-ion battery. J Energy Storage 2020;28:101242.

[191] Guan T, Sun S, Yu F, Gao Y, Fan P, Zuo P, Du C, Yin G. The degradation of $LiCoO_2$/graphite batteries at different rates. Electrochim Acta 2018;279:204–12.

[192] Omar N, Monem MA, Firouz Y, Salminen J, Smekens J, Hegazy O, Gaulous H, Mulder G, Van den Bossche P, Coosemans T, et al. Lithium iron phosphate based battery–assessment of the aging parameters and development of cycle life model. Appl Energy 2014;113:1575–85.

[193] Waldmann T, Wohlfahrt-Mehrens M. Effects of rest time after li plating on safety behavior—ARC tests with commercial high-energy 18650 Li-ion cells. Electrochim Acta 2017;230:454–60.

[194] Yang L, Cheng X, Gao Y, Ma Y, Zuo P, Du C, Cui Y, Guan T, Lou S, Wang F, et al. Lithium deposition on graphite anode during long-term cycles and the effect on capacity loss. RSC Adv 2014;4:26335–41.

[195] Lu Y, Zhu T, McShane E, McCloskey BD, Chen G. Single-crystal $LiNi_xmn_yco_{1-x-y}O_2$ cathodes for extreme fast charging. Small 2022;18:2105833.

[196] Meng F, Xiong X, Tan L, Yuan B, Hu R. Strategies for improving electrochemical reaction kinetics of cathode materials for subzero-temperature Li-ion batteries: a review. Energy Storage Mater 2022;44:390–407.

[197] Hildebrand S, Rheinfeld A, Friesen A, Haetge J, Schappacher FM, Jossen A, Winter M. Thermal analysis of $LiNi_{0.4}co_{0.2}mn_{0.4}O_2$/mesocarbon microbeads cells and electrodes: state-of-charge and state-of-health influences on reaction kinetics. J Electrochem Soc 2018;165:A104.

[198] Wu Z, Zhang C, Yuan F, Lyu M, Yang P, Zhang L, Zhou M, Wang L, Zhang S, Wang L. Ni-rich cathode materials for stable high-energy lithium-ion batteries. Nano Energy 2024;126:109620.

[199] Wu X, Bai Y, Li Z, Liu J, Zhao K, Du Z. Effects of charging rates on $LiNi_{0.6}mn_{0.2}co_{0.2}O_2$ (NMC622)/graphite Li-ion cells. J Energy Chem 2021;56:121–6.

[200] Gohar GA, An L, Ali HM, Zhao H. A study on chemical kinetics of carbonates-based electrolytes for enhancing fire safety in lithium-ion batteries–a review. J Energy Storage 2025;131:117492.

[201] Fleischhammer M, Waldmann T, Bisle G, Hogg B-I, Wohlfahrt-Mehrens M. Interaction of cyclic ageing at high-rate and low temperatures and safety in lithium-ion batteries. J Power Sources 2015;274:432–9.

[202] Huang Y, Zhao Y, Bai W, Cao Y, Xu W, Shen X, Wang Z. Study on the influence of high rate charge and discharge on thermal runaway behavior of lithium-ion battery. Process Saf Environ Prot 2024;191:1483–94.

[203] Ouyang D, Liu B, Huang J, Wang Z. Degradation and safety performance of lithium-ion cells under high-rate charging/discharging scenarios. Process Saf Environ Prot 2024;185:76–85.

[204] Zhang L, Liu L, Terekhov A, Warnberg D, Zhao P. Thermal runaway of Li-ion battery with different aging histories. Process Saf Environ Prot 2024;185:910–7.

[205] Huang Y, Shen X, Zhao Y, Wang J, Cao Y, Bai W, Fan Y, Lu Y, Wang Z. Investigation on the inhibition mechanism of thermal runaway propagation in high-rate cycling lithium-ion pouch cells. Process Saf Environ Prot 2025;197:106975.

[206] Zhang G, Wei X, Wang X, Chen S, Zhu J, Dai H. Evolution mechanism and non-destructive assessment of thermal safety for lithium-ion batteries during the whole lifecycle. Nano Energy 2024;126:109621.

[207] Guo Y, Cai J, Liao Y, Hu J, Zhou X. Insight into fast charging/discharging aging mechanism and degradation-safety analytics of 18650 lithium-ion batteries. J Energy Storage 2023;72:108331.

[208] Ji C, Liu D, Liu Y, Wang S, Wang Y, Zhang Z, Wang B. Effect of low temperature and high-rate cyclic aging on thermal characteristics and safety of lithium-ion batteries. Process Saf Environ Prot 2024;188:1514–26.

[209] Lyu S, Li N, Sun L, Jiao S, Chen H, Song W-L. Rapid operando gas monitor for commercial lithium ion batteries: gas evolution and relation with electrode materials. J Energy Chem 2022;72:14–25.

[210] Song M, Choe S-Y. Fast and safe charging method suppressing side reaction and lithium deposition reaction in lithium ion battery. J Power Sources 2019;436:226835.

[211] Wang L, Zhuo L, Zhang C, Zhao F. Carbon dioxide-induced homogeneous deposition of nanometer-sized cobalt ferrite ($CoFe_2O_4$) on graphene as high-rate and cycle-stable anode materials for lithium-ion batteries. J Power Sources 2015;275:650–9.

[212] Liu S, Li K, Yu J. Battery pack condition monitoring and characteristic state estimation: challenges, techniques, and future prospectives. J Energy Storage 2025;105:114446.

[213] Baronti F, Roncella R, Saletti R. Performance comparison of active balancing techniques for lithium-ion batteries. J Power Sources 2014;267:603–9.

[214] Zhong H, Zhong Q, Yang J, Zhong S. Thermal behavior and failure mechanisms of 18650 lithium ion battery induced by overcharging cycling. Energy Rep 2022;8:7286–96.

[215] Guo Z, Ma Z, Zhao W, Wang S, Zhao H, Ren L. Quantitative investigation on the overcharge cycling-induced severe degradation of electrochemical and mechanical properties of lithium-ion battery cells. Energy 2025;318:134900.

[216] Zhao W, Ma Z, Guo Z, Wang S, Liu J, Cai X, Zhao H, Ren L. Investigation on overcharge cycling-induced degradation of lithium-ion batteries and mechanical deterioration of components. J Power Sources 2025;654:237864.

[217] Liu J, Duan Q, Peng W, Feng L, Ma M, Hu S, Sun J, Wang Q. Slight overcharging cycling failure of commercial lithium-ion battery induced by the jelly roll destruction. Process Saf Environ Prot 2022;160:695–703.

[218] Zhang Z, Ji C, Wang Y. Failure mechanism and thermal runaway in batteries during micro-overcharge aging at different temperatures. Materials 2024;17:2125.

[219] Guo Z, Zhao W, Ma Z, Wang S, Liu J, Zhao H, Ren L. Slight overdischarge cycling-induced severe degradation of electrochemical and mechanical properties of lithium-ion batteries. Appl Energy 2025;393:126101.

[220] Erol S, Orazem ME, Muller RP. Influence of overcharge and over-discharge on the impedance response of $LiCoO_2$ | C batteries. J Power Sources 2014;270:92–100.

[221] Guo R, Lu L, Ouyang M, Feng X. Mechanism of the entire overdischarge process and overdischarge-induced internal short circuit in lithium-ion batteries. Sci Rep 2016;6:30248.

[222] Maleki H, Howard JN. Effects of overdischarge on performance and thermal stability of a Li-ion cell. J Power Sources 2006;160:1395–402.

[223] Guo Z, Yang S, Zhao W, Wang S, Liu J, Ma Z, Zhao H, Ren L. Overdischarge-induced evolution of cu dendrites and degradation of mechanical properties in lithium-ion batteries. J Energy Chem 2023;78:497–506.

[224] Mukai K, Inoue T, Hasegawa M. Rationalizing thermal reactions of C_6li_x negative electrode with nonaqueous electrolyte. J Power Sources 2017;366:185–92.

[225] Wang Y, Jiang J, Dahn J. The reactivity of delithiated $li(ni_{1/3}co_{1/3}MN_{1/3})o_2$, $li(ni_{0.8}co_{0.15}al_{0.05})o_2$ or $LiCoO_2$ with non-aqueous electrolyte. Electrochem Commun 2007;9:2534–40.

[226] Ouyang M, Ren D, Lu L, Li J, Feng X, Han X, Liu G. Overcharge-induced capacity fading analysis for large format lithium-ion batteries with $li_yni_{1/3}co_{1/3}MN_{1/3}O_2 + li_ymn_2O_4$ composite cathode. J Power Sources 2015;279:626–35.

[227] Xie S, Gong Y, Ping X, Sun J, Chen X, He Y. Effect of overcharge on the electrochemical and thermal safety behaviors of $LiNi_{0.5}mn_{0.3}co_{0.2}O_2$/graphite lithium-ion batteries. J Energy Storage 2022;46:103829.

[228] Liu J, Duan Q, Feng L, Ma M, Sun J, Wang Q. Capacity fading and thermal stability of $LiNi_xco_ymn_zO_2$/graphite battery after overcharging. J Energy Storage 2020;29:101397.

[229] Zhang L, Ma Y, Cheng X, Cui Y, Guan T, Gao Y, Du C, Yin G, Lin F, Nordlund D. Degradation mechanism of over-charged $LiCoO_2$/mesocarbon microbeads battery during shallow depth of discharge cycling. J Power Sources 2016;329:255–61.

[230] Zhang G, Wei X, Chen S, Zhu J, Han G, Tang X, Hua W, Dai H, Ye J. Comprehensive investigation of a slight overcharge on degradation and thermal runaway behavior of lithium-ion batteries. ACS Appl Mater Interfaces 2021;13:35054–68.

[231] Yang M, Ye Y, Yang A, Jiang Z, Wang X, Yuan H, Rong M. Comparative study on aging and thermal runaway of commercial $LiFePO_4$/graphite battery undergoing slight overcharge cycling. J Energy Storage 2022;50:104691.

[232] Huang P, Zeng G, He Y, Liu S, Li E, Bai Z. Damage evolution mechanism and early warning using long short-term memory networks for battery slight overcharge cycles. Renew Energy 2023;217:119171.

[233] Yu Y, Ping P, Wang G, Guo J, Feng Z, Gao W, Liu K, Kong D. Experimental study on expansion force characteristics of $LiFePO_4$ battery under overcharge cycles. Appl Energy 2025;399:126498.

[234] Liu J, Peng W, Yang M, Jin K, Liu P, Sun J, Wang Q. Quantitative analysis of aging and detection of commercial 18650 lithium-ion battery under slight overcharging cycling. J Clean Prod 2022;340:130756.

[235] Zhang L, Huang L, Zhang Z, Wang Z, Dorrell DD. Degradation characteristics investigation for lithium-ion cells with NCA cathode during overcharging. Appl Energy 2022;327:120026.

[236] Ren D, Feng X, Lu L, Ouyang M, Zheng S, Li J, He X. An electrochemical-thermal coupled overcharge-to-thermal-runaway model for lithium ion battery. J Power Sources 2017;364:328–40.

[237] Sun P, Zhang X, Wang S, Zhu Y. Lithium-ion battery degradation caused by overcharging at low temperatures. Therm Sci Eng Prog 2022;30:101266.

[238] Liu Y, Mao G, Yang M, Jiang J, Jiang J. Slight overcharge aging behaviors and thermal runaway characteristics of $li(ni_{0.5}co_{0.2}mn_{0.3})o_2$/graphite batteries at different ambient temperatures. ACS Appl Energy Mater 2023;6:6760–72.

[239] Feng L, Jiang L, Liu J, Wang Z, Wei Z, Wang Q. Dynamic overcharge investigations of lithium ion batteries with different state of health. J Power Sources 2021;507:230262.

[240] Zhang G, Wei X, Chen S, Zhu J, Han G, Dai H. Revealing the impact of slight electrical abuse on the thermal safety characteristics for lithium-ion batteries. ACS Appl Energy Mater 2021;4:12858–70.

[241] Guo Z, Ma Z, Liu J, Zhao W, Wang S, Zhao H, Ren L. Overcharging cycle aging-induced severe degradation of safety properties of lithium-ion pouch battery cells subjected to mechanical abuse. Energy 2025;320:135168.

[242] Ouyang D, Weng J, Chen M, Wang J, Wang Z. Investigation on topographic, electrochemical and thermal features of aging lithium-ion cells induced by overcharge/over-discharge cycling. J Energy Storage 2023;68:107799.

[243] Li C, Liu X, Wang C, Ye L, Wu T, Liang Z, Zhang Z, Zeng Y, Li K. Electrochemical-thermal behaviors of retired power lithium-ion batteries during high-temperature and overcharge/over-discharge cycles. Case Stud Therm Eng 2024;61:104898.

[244] Yang X, Wang Z, Xie S. Influence of overdischarge depth on the aging and thermal safety of $LiNi_{0.5}co_{0.2}mn_{0.3}O_2$/Graphite cells. Battery Energy 2025;e70008.

[245] Ouyang D, Weng J, Chen M, Wang J, Wang Z. Sensitivities of lithium-ion batteries with different capacities to overcharge/over-discharge. J Energy Storage 2022;52:104997.

[246] Yin T, Jia L, Li X, Zheng L, Dai Z. Effect of high-rate cycle aging and over-discharge on NCM811 ($LiNi_{0.8}co_{0.1}mn_{0.1}O_2$) batteries. Energies 2022;15:2862.

[247] Wang Z, Zhu L, Liu J, Wang J, Yan W. Gas sensing technology for the detection and early warning of battery thermal runaway: a review. Energy Fuels 2022;36:6038–57.

[248] Liao Y, Zhang H, Peng Y, Hu Y, Liang J, Gong Z, Wei Y, Yang Y. Electrolyte degradation during aging process of lithium-ion batteries: mechanisms, characterization, and quantitative analysis. Adv Energy Mater 2024;14:2304295.

[249] Liu X, Wu J, Fan C, Zhang Y, Quan W, Li J, Hu N, Yang J, Zeng M, Yang Z. One-dimensional conductive metal–organic frameworks enable real-time chemiresistive detection of thermal runaway gases. ACS Sens 2025;10:6464–75.
[250] Daniels RK, Kumar V, Chouhan SS, Prabhakar A. Thermal runaway fault prediction in air-cooled lithium-ion battery modules using machine learning through temperature sensors placement optimization. Appl Energy 2024;355:122352.
[251] Zhang J, Li Y, Ma L. Study on the effect of aging on thermal runaway behavior of lithium-ion batteries under different heating positions. Appl Therm Eng 2025;127793.
[252] Chu Y, Mu Y, Zou L, Wu F, Yang L, Feng Y, Zeng L. Oxygen release in ni-rich layered cathode for lithium-ion batteries: mechanisms and mitigating strategies. Chemelectrochem 2024;11:e202300653.
[253] Doose S, Hahn A, Fischer S, Müller J, Haselrieder W, Kwade A. Comparison of the consequences of state of charge and state of health on the thermal runaway behavior of lithium ion batteries. J Energy Storage 2023;62:106837.
[254] Cai T, Valecha P, Tran V, Engle B, Stefanopoulou A, Siegel J. Detection of Li-ion battery failure and venting with CO_2 sensors. eTransportation 2021;7:100100.
[255] Fernandes Y, Bry A, De Persis S. Identification and quantification of gases emitted during abuse tests by overcharge of a commercial Li-ion battery. J Power Sources 2018;389:106–19.
[256] Teng Z, Lv C. Detection toward early-stage thermal runaway gases of Li-ion battery by semiconductor sensor. Front Chem 2025;13:1586903.
[257] Pu Z, Yang M, Jiao M, Zhao D, Huo Y, Wang Z. Thermal runaway warning of lithium battery based on electronic nose and machine learning algorithms. Batteries 2024;10:390.
[258] Luo L, Chen J, Hui AG, Liu R, Zhou Y, Liang H, Wang Z, Luo H, Fang F. Highly sensitive non-dispersive infrared gas sensor with innovative application for monitoring carbon dioxide emissions from lithium-ion battery thermal runaway. Micromachines 2024;16:36.
[259] Zhang Y, Li S, Mao B, Shi J, Zhang X, Zhou L. A multi-level early warning strategy for the LiFePO4 battery thermal runaway induced by overcharge. Appl Energy 2023;347:121375.
[260] Huang W, Ye Y, Chen H, Vilá RA, Xiang A, Wang H, Liu F, Yu Z, Xu J, Zhang Z, et al. Onboard early detection and mitigation of lithium plating in fast-charging batteries. Nat Commun 2022;13:7091.
[261] Xu W, Li L, Shi F, Chen Q. Ultrasonic spectroscopy for in situ early detection and dynamic monitoring of lithium plating in lithium-ion batteries. Cell Rep Phys Sci 2025;6.
[262] Jin Y, Zheng Z, Wei D, Jiang X, Lu H, Sun L, Tao F, Guo D, Liu Y, Gao J, et al. Detection of micro-scale li dendrite via H_2 gas capture for early safety warning. Joule 2020;4:1714–29.
[263] Cai T, Stefanopoulou AG, Siegel JB. Early detection for Li-ion batteries thermal runaway based on gas sensing. ECS Trans 2019;89:85.
[264] Wang C-Y, Qin K, Ge S, Gupta N, Sasaki T, Aotani K. Metrics for evaluating safe electrolytes in energy-dense lithium batteries. Nat Energy 2025;10:1382–90.
[265] Liu C, Dai H, Wang D, Ren X, Lyu S, Fan J, Lv S, Zhu S, Li N, Wang Y. Understanding thermal runaway in lithium-ion batteries: trigger, mechanism, and early warning strategies. J Electrochem Soc 2024;171:120527.
[266] Stockhausen R, Gehrlein L, Müller M, Bergfeldt T, Hofmann A, Müller FJ, Maibach J, Ehrenberg H, Smith A. Investigating the dominant decomposition mechanisms in lithium-ion battery cells responsible for capacity loss in different stages of electrochemical aging. J Power Sources 2022;543:231842.
[267] Jiang Z, Zhang L, Yu Y, Zou J, Kim F. The resurging of hydrocarbon gas as early sign of battery rollover degradation. ACS Appl Mater Interfaces 2025;17:4934–40.
[268] Velumani D, Bansal A. Thermal behavior of lithium-and sodium-ion batteries: a review on heat generation, battery degradation, thermal runway–perspective and future directions. Energy Fuels 2022;36:14000–29.
[269] Zhang Y, Ping P, Dai X, Li C, Li Z, Zhuo P, Tang L, Kong D, Yin X. Failure mechanism and thermal runaway behavior of lithium-ion battery induced by arc faults. Renew Sustain Energy Rev 2025;207:114914.
[270] Abbas SM, Gstrein G, Jauernig AD, Schmid A, Michelini E, Hinterberger M, Ellersdorfer C. Influence of lithium plating on the mechanical properties of automotive High-Energy pouch batteries. Batteries 2025;11:330.
[271] Kwon B, Schraiber A, Jeevarajan JA. Evaluating fire and smoke risks with lithium-ion cells, modules, and batteries. ACS Energy Lett 2024;9:5319–28.
[272] Jia Y, Li J, Yao W, Li Y, Xu J. Precise and fast safety risk classification of lithium-ion batteries based on machine learning methodology. J Power Sources 2022;548:232064.
[273] Naha A, Khandelwal A, Agarwal S, Tagade P, Hariharan KS, Kaushik A, Yadu A, Kolake SM, Han S, Oh B. Internal short circuit detection in Li-ion batteries using supervised machine learning. Sci Rep 2020;10:1301.
[274] Xie J, Zhang L, Yao T, Li Z. Quantitative diagnosis of internal short circuit for cylindrical Li-ion batteries based on multiclass relevance vector machine. J Energy Storage 2020;32:101957.
[275] Liu S, Guo Q, Zhang J, Huang Z, Han D. Investigation on thermal runaway behaviors and gas generation dynamics of lithium-ion batteries induced by electrical abuse at low-pressure conditions. J Energy Storage 2025;125:116855.
[276] Park S, Pozzi A, Whitmeyer M, Perez H, Kandel A, Kim G, Choi Y, Joe WT, Raimondo DM, Moura S. A deep reinforcement learning framework for fast charging of Li-ion batteries. IEEE Trans Transp Electrif 2022;8:2770–84.
[277] Unagar A, Tian Y, Chao MA, Fink O. Learning to calibrate battery models in real-time with deep reinforcement learning. Energies 2021;14:1361.
[278] Li W, Cui H, Nemeth T, Jansen J, Ünlübayir C, Wei Z, Feng X, Han X, Ouyang M, Dai H, et al. Cloud-based health-conscious energy management of hybrid battery systems in electric vehicles with deep reinforcement learning. Appl Energy 2021;293:116977.
[279] Schmid M, Kneidinger H-G, Endisch C. Data-driven fault diagnosis in battery systems through cross-cell monitoring. IEEE Sens J 2020;21:1829–37.
[280] Qiao D, Wei X, Fan W, Jiang B, Lai X, Zheng Y, Tang X, Dai H. Toward safe carbon–neutral transportation: battery internal short circuit diagnosis based on cloud data for electric vehicles. Appl Energy 2022;317:119168.
[281] Xue Q, Li G, Zhang Y, Shen S, Chen Z, Liu Y. Fault diagnosis and abnormality detection of lithium-ion battery packs based on statistical distribution. J Power Sources 2021;482:228964.
[282] Firoozi R, Sattarzadeh S, Dey S. Cylindrical battery fault detection under extreme fast charging: a physics-based learning approach. IEEE Trans Energy Convers 2021;37:1241–50.
[283] Ji W, Deng S. Autonomous discovery of unknown reaction pathways from data by chemical reaction neural network. J Phys Chem A 2021;125:1082–92.
[284] Zhang J, Ma C, Liu S, Guo Q, Liu S, Han P, Huang Z, Han D. Chemical reaction neural networks to map lithium-ion battery thermal runaway gas generation. Cell Rep Phys Sci 2025;6:102563.
[285] Zhao J, Ling H, Wang J, Burke AF, Lian Y. Data-driven prediction of battery failure for electric vehicles. iScience 2022;25:104172.
[286] Zhou Z-H, Li M. Semi-supervised learning by disagreement. Knowl Inf Syst 2010;24:415–39.
[287] Raissi M, Perdikaris P, Karniadakis GE. Physics-informed neural networks: a deep learning framework for solving forward and inverse problems involving nonlinear partial differential equations. J Comput Phys 2019;378:686–707.
[288] Nascimento RG, Corbetta M, Kulkarni CS, Viana FA. Hybrid physics-informed neural networks for lithium-ion battery modeling and prognosis. J Power Sources 2021;513:230526.
[289] Shi D, Zhao J, Eze C, Wang Z, Wang J, Lian Y, Burke AF. Cloud-based artificial intelligence framework for battery management system. Energies 2023;16:4403.
[290] Huang J, Boles ST, Tarascon J-M. Sensing as the key to battery lifetime and sustainability. Nat Sustain 2022;5:194–204.
[291] Finegan DP, Darst J, Walker W, Li Q, Yang C, Jervis R, Heenan TM, Hack J, Thomas JC, Rack A, et al. Modelling and experiments to identify high-risk failure scenarios for testing the safety of lithium-ion cells. J Power Sources 2019;417:29–41.
[292] Zhang S, Zhu X, Qiu J, Xu C, Wang Y, Feng X. Modeling and simulation of a gas-exhaust design for battery thermal runaway propagation in a LiFePO4 module. Batteries 2024;10:176.
[293] Wang G, Kong D, Ping P, He X, Lv H, Zhao H, Hong W. Modeling venting behavior of lithium-ion batteries during thermal runaway propagation by coupling CFD and thermal resistance network. Appl Energy 2023;334:120660.
[294] Li W, León Quiroga V, Crompton K, Ostanek JK. High resolution 3-D simulations of venting in 18650 lithium-ion cells. Front Energy Res 2021;9:788239.
[295] Li W, Ostanek J. Heat transfer experiments and correlations for vent gases emerging from a Li-ion battery and impinging on a flat surface. Int J Heat Mass Transf 2023;200:123516.
[296] Mateev V, Marinova I, Kartunov Z. Automatic system for Li-ion battery packs gas leakage detection. In: 2018 12th international conference on sensing technology (ICST). IEEE; 2018. p. 13–16.
[297] Aykol M, Herring P, Anapolsky A. Machine learning for continuous innovation in battery technologies. Nat Rev Mater 2020;5:725–7.